

Network Geometry

Marián Boguñá,^{1,2} Ivan Bonamassa,³ Manlio De Domenico,^{4,*}
Shlomo Havlin,³ Dmitri Krioukov,^{5,6} and M. Ángeles Serrano^{1,2,7}

¹*Departament de Física de la Matèria Condensada,*

Universitat de Barcelona, Martí i Franquès 1, E-08028 Barcelona, Spain

²*Universitat de Barcelona Institute of Complex Systems (UBICS), Universitat de Barcelona, Barcelona, Spain*

³*Department of Physics, Bar-Ilan University, 52900 Ramat-Gan, Israel*

⁴*CoMuNe Lab, Fondazione Bruno Kessler, Via Sommarive 18, 38123 Povo (TN), Italy*

⁵*Network Science Institute, Northeastern University,*

177 Huntington Avenue, Boston, MA, 02215

⁶*Department of Physics, Department of Mathematics,*

Department of Electrical & Computer Engineering, Northeastern University,

110 Forsyth Street, 111 Dana Research Center, Boston, MA 02115, USA

⁷*ICREA, Passeig Lluís Companys 23, E-08010 Barcelona, Spain*

(Dated: July 6, 2022)

Networks are natural geometric objects. Yet the discrete metric structure of shortest path lengths in a network, known as chemical distances, is definitely not the only reservoir of geometric distances that characterize many networks. The other forms of network-related geometries are the geometry of continuous latent spaces underlying many networks, and the effective geometry induced by dynamical processes in networks. A solid and rapidly growing amount of evidence shows that the three approaches are intimately related. Network geometry is immensely efficient in discovering hidden symmetries, such as scale-invariance, and other fundamental physical and mathematical properties of networks, as well as in a variety of practical applications, ranging from the understanding how the brain works, to routing in the Internet. Here, we review the most important theoretical and practical developments in network geometry in the last two decades, and offer perspectives on future research directions and challenges in this novel frontier in the study of complexity.

Many of the existing analytical and computational tools for the analysis of complex networks emerged from classical methods in statistical physics [1]. Over the years, this approach has proven essential for identifying microscopic models capable of reproducing the structural properties observed in many real-world networks [2–4], and to accurately quantify their influence on collective and critical phenomena [5–8]. Recently, other complementary approaches have been employed to study networks from different perspectives [9, 10] leading to novel fundamental insights. One such approach is *geometry*, the focus of this review.

From the physics perspective, early evidence that complex networks possess some nontrivial geometric properties appeared with the discovery of their *self-similarity* under suitable scale transformations [11], a result that has pushed the scientific interest towards two major geometric approaches. Initially, *fractal geometry* was the major reservoir of methods and ideas. Besides boosting the study of transport [12, 13] in complex media, the fractal geometric paradigm has inspired the definition of a (reversible) graph-theoretical renormalization procedure that has helped researchers to classify networks into universality classes [14, 15], as well as better understanding the growth mechanisms [16] lurking in their temporal evolution.

Along the lines of this initial success, it was later found [17] that network self-similarity can be explained on a more fundamental level in terms of a latent *hyperbolic geometry* underlying their structure. This hidden metric space approach has proved successful for explaining, within a unique framework, the most common

structural properties of many real networks [17, 18], their navigability [19, 20], and their community [21–23] and multiscale structure [24]. Furthermore, since the group of symmetries of hyperbolic spaces is the familiar Lorentz group, the latent hyperbolicity of networks has been advocated to explain not only their structural self-similarity, but also the dynamical laws of their growth [25–27], establishing certain duality relations reminiscent of the AdS/CFT correspondence [28].

In light of these advances, it is not surprising that the geometric approach is rapidly leading to many useful practical applications and novel theoretical insights. In the context of information or epidemic spreading, for example, the adoption of transport-based metrics and of the corresponding *diffusion geometries* [29] is helping unfolding the spatiotemporal evolution of network-driven dynamical processes [30, 31], opening new research directions [32, 33] in many neighboring areas of science.

Contextually to these approaches, the mathematical perspective has further expanded the frontiers of network geometry with new questions and methods. In this context, a fundamental challenge is the characterization of networks' *curvature* [34, 35], in which respect combinatorial approaches [36] and manifold embeddings [37] have been adopted. While there exist very different definitions of networks curvature, and no established consensus which one is the most appropriate, these approaches have disclosed profound connections between network measures – in particular the graph Laplacian – with exquisitely geometrical quantities such as the Laplace-Beltrami operator in Riemannian manifolds [38, 39], or the Fisher-Rao metric [40] in Information Geometry, whose study is just at its infancy.

The net result of such profound developments is an

*Corresponding author: mdedomenico@fbk.eu

unprecedented cross-fertilization among many diverse areas of natural sciences. Notably, the field of *emergent geometries* [41, 42], aiming to generate networks endowed with hidden geometric manifolds without using underlying spaces, is gaining momentum due to its intimate connection with longstanding combinatoric problems in many approaches to quantum gravity, such as *causal sets* [43, 44], *quantum graphity* [45] and *causal dynamic triangulations* [46].

This rapid interdisciplinary progress suggests that now is about a right time to ground a milestone in network geometry research, from where to ponder on future challenges. Here, we review three major research directions in network geometry: the self-similar fractal geometry of network structure (Sec. I), the hyperbolic geometry of networks' latent spaces (Sec. II), and the geometry induced by dynamic processes, such as diffusion, in networks (Sec. III). Distances are all different in the three geometries, yet intimately related. They are, respectively, the *chemical distances*, i.e. the hop lengths of shortest paths in a network, the *similarity distances*, i.e. the distances between network nodes in a latent space, and the *diffusion distances*, e.g. emerging from some spreading dynamics in a network. We conclude the review with the discussion in Sec. IV of current advances in network geometry in a broader perspective, focusing on the most interesting open challenges, both theoretical and those that arise in applications, with the aim of emphasizing their rising impacts in physics and other fields of science.

I. FRACTAL GEOMETRY OF NETWORK STRUCTURE

Self-similarity is a characteristic of certain geometric objects, known as fractals [49], expressing the invariance of their forms under rescaling. From snowflakes and ferns to critical phenomena near phase transitions [50, 51], this *scale-free* property is ubiquitous among many natural systems whose scaling factors are typically the length scales defined by the metric space where they are naturally embedded. In the context of complex networks, a similar discovery was made, though referring to the absence of a characteristic number of links k per node rather than a length scale, as described by a fat-tailed degree distribution of the form $P(k) \sim k^{-\gamma}$ as $k \gg 1$, with $\gamma \in (2, 3)$. If, on one side, this scale-free property hinted at the existence of a structural invariance under a suitable length-scale transform, the equally ubiquitous *small-world* property, i.e. an average geodesic path $\bar{\ell}$ between nodes growing logarithmically or slower [52] with the system's size N , contextually hindered this possibility – implying a diverging Hausdorff dimension d_f – and led to the common belief that networks cannot be self-similar. Fortunately, this apparent contradiction proved to be a very prolific problem, whose analysis throughout tools of *fractal geometry* [53] has yielded many significant insights into the scaling, renormalization and universality of complex networks.

Chemical scaling and renormalization. In the graph theoretical sense, the number ℓ of edges along any

shortest path connecting two nodes is a well-defined metric, a.k.a. the *chemical distance* [54], which can be adopted to observe networks at different length scales. In this respect, Song *et al.* [11] have shown that the process of zooming out on networks can be performed analogously to that of regular fractals by finding an optimal covering of nodes via non-overlapping boxes of size ℓ_B . This chemical tiling induces a natural rescaling of the network's structure (Box, panel A), whose iteration generates a series of coarse-grained networks based on the box length ℓ_B . By applying this chemical-space renormalization group (RG) transformation [55, 56], a surprisingly large variety of real-world and synthetic networks result in being *statistically self-similar*, in the sense that their degree distribution [11] and degree correlations [57] remain invariant (Fig. 1a,b) over the available length scales.

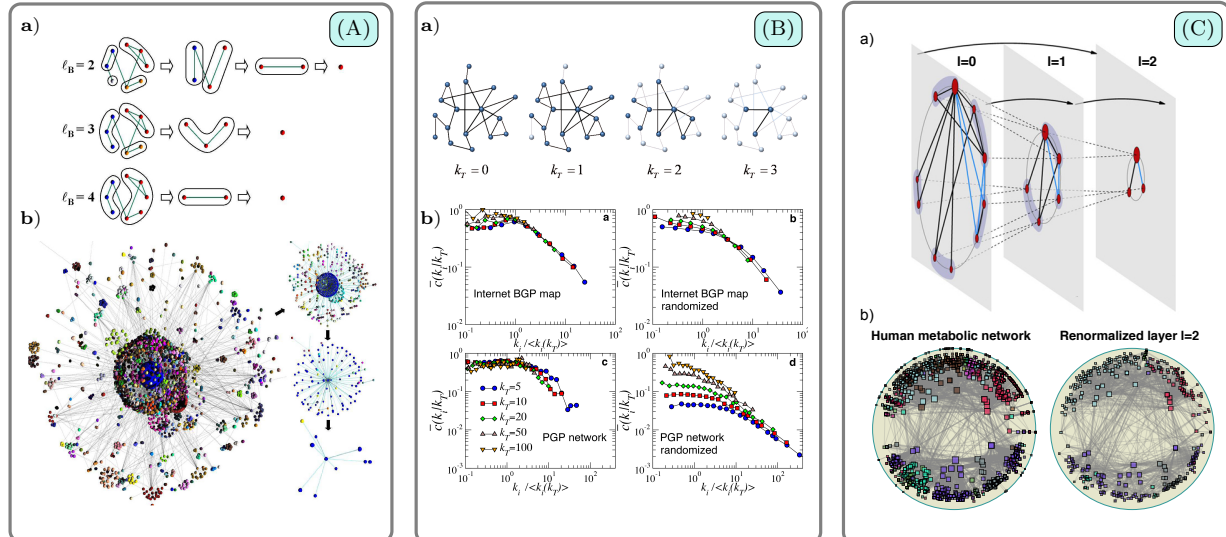
A primary consequence of this discovery was the characterization of self-similar networks according to a set of *fractal dimensions* [59] whose scaling relations were proved to be fundamental for understanding the networks' organization, their evolution and, more importantly, their functioning. In what follows we introduce the reader to an essential selection of such dimensions, and discuss their relation to the large-organization of the corresponding systems. Let us first notice that a crucial rule in the fractal analysis of the networks' scale-invariant observables is played by the rescaling of the number of boxes (supernodes) N' and of the degree of each box k' under each renormalization step, \mathcal{R}_b , respectively given by

$$N \xrightarrow{\mathcal{R}_b} N' \sim \ell_B^{-d_B} N, \quad k \xrightarrow{\mathcal{R}_b} k' \sim \ell_B^{-d_k} k, \quad (1)$$

where d_B, d_k define respectively the *box dimension* and the *degree dimension* of the self-similar network. By combining the fractal scaling above with the invariance of $P(k)$, it can be shown [11] that the exponents d_B, d_k and γ are not independent, as they obey the relation $\gamma = 1 + d_B/d_k$. This result led to identify two broad families of self-similar networks [60, 61]: *i) pure fractals* (such as biological networks, the WWW or social networks) if d_B, d_k are both finite, and *ii) pure small-worlds* (such as the Internet at the router level, or synthetic networks) when $d_B, d_k \rightarrow \infty$ (Fig. 1c), implying an exponential decay in place of Eq. (1).

Such dichotomy can be understood by analyzing the different profiles in the connectivity correlations [11, 62]: fractal architectures, in fact, feature a strong “hub-hub repulsion” (*disassortativity*) that makes them more dispersed than pure small-worlds. Following this lead, the analysis of structural correlation in networks significantly benefited from the discovery of self-similarity. For example, in Ref. [57] the scale-invariant observable, $E(k) := \int_k^\infty P(k|k')dk' / \int_k^\infty P(k')dk' \sim k^{-(\epsilon-\gamma)}$ where $P(k|k')$ is the conditional degree-probability and $\epsilon > 1$, was introduced to characterize degree correlations (Fig. 1b) through a single exponent. Turning to the renormalization scheme, this quantity was found to be related with the probability that boxes are connected through their hubs, whose scaling factor $\mathcal{E}(\ell_B) \sim \ell_B^{-d_e}$ defines the *hub-hub dimension* d_e (Fig. 1c, lower inset). Arguments similar to those adopted for the triple (d_B, d_k, γ)

Box: ZOOMING OUT ON COMPLEX NETWORKS



(A) **Chemical-space renormalization.** a). Demonstration of the box covering technique [11]. The original network (first column) is tiled with the minimum number of chemical boxes of given diameter ℓ_B – using e.g. the Maximum Excluded Mass Burning (MEMB) algorithm [47] – so that all nodes within a box are at a distance smaller than ℓ_B . The renormalized network (second column) is then built by replacing each box with supernodes, which are connected if there is at least one link between the unrenormalized boxes. This coarse graining is repeatedly applied – though for a limited number of steps due to small-worldness – until the network is reduced to a single “ancestral” node. b). Three chemical-space RG steps applied to the entire WWW for a fixed box length $\ell_B = 3$ [11]. The network’s structure remains statistically invariant under chemical-RG (see Fig. 1). (B) **Degree-thresholding renormalization.** a) Subgraphs are obtained by removing all nodes with degrees below a given threshold k_T . This defines a hierarchy of nested subgraphs that are found to be self-similar in real complex networks. b) Data collapse of the clustering spectrum of the different subgraphs for the Internet and Border Gateway Protocol graphs (left column) and their randomized versions preserving the degree sequence (right column), for which the collapse is destroyed. The nice collapse of the clustering spectrum for real complex networks finds a natural explanation in their underlying geometry [17]. (C) **Geometric renormalization.** a) Similarly to A), the renormalization transformation zooms out by changing the minimum length scale from that of the original network to a larger value, this time in the similarity space [48]. First, non-overlapping blocks of consecutive nodes are defined along the similarity circle. Second, the blocks are coarse-grained into supernodes. Each supernode is then placed within the angular region defined by the corresponding block so that the order of nodes is preserved. Finally, two supernodes are connected if any of their constituents were in the precursor layer. b) Hyperbolic embedding of the human metabolic network and its renormalized layer $l = 2$ [48]. The colours of the nodes correspond to the community structure detected by the Louvain algorithm. Notice how the renormalized network preserves the original community structure despite being four times smaller.

lead [57] to the scaling relation $\epsilon = 2 + d_e/d_k$, implying that $\epsilon > 2$ for any fractal networks. Armed with these results, it proved possible to classify a large variety of networks according to their scale-invariant features, as shown in the (γ, ϵ) -diagram in Fig. 1d.

Functional modularity and evolution. If on one side the RG process unveiled the large-scale organization of self-similar networks, on another it opened a window into the analysis of their meso-scale architecture. The chemical RG transformation, in fact, naturally generates a hierarchy of modular configurations into which a given network can be *optimally* partitioned at increasing length scales ℓ_B . The invariant character of this tiling can be quantified through the power-law scaling $Q(\ell_B) \sim \ell_B^{d_M}$ [12, 63], where d_M is the *modular dimension* and $Q(\ell_B)$ is a variation of the standard modularity factor [64, 65] which is maximized by the box covering. In particular, a value of $d_M = 1$ (characteristic of regular lattices) represents the borderline case separating modular ($d_M > 1$) from random non-modular networks ($d_M < 1$). In this perspective, biological networks typically show pronounced modularity patterns (i.e., large d_M), in contrast with small-world-dominated structures (like e.g. the prefer-

ential attachment (PA) model, or configuration model networks) where d_M typically vanishes [12].

These results raised some puzzles of interpretation. Besides questioning the functional significance encoded in the modules detected by the RG, they advanced the fundamental problem about the growth mechanisms leading to their emergence, a task with respect to which popular rules like the “rich-get-richer” principle of PA, or the “democratic” wiring of Erdős-Rényi (ER) networks, did not succeed. The first issue was soon clarified by analyzing diverse biological networks [12, 16, 63] with known biochemical annotations. In this case, the chemical RG proved to detect modules as accurately as other clustering algorithms [64, 65]. This is best manifested in Ref. [63], where the modular detection by chemical RG resulted into the first, integrated multiscale-view of the network of human cell differentiation (Fig. 2(A)a,b), hinting at the perspective of identifying hitherto unknown functional relations between previously unrelated cellular domains.

The problem of growth, instead, benefited from the correlation analysis of self-similar networks. Modularity, in fact, spontaneously emerges from structural fractality (though the converse is not necessarily true)

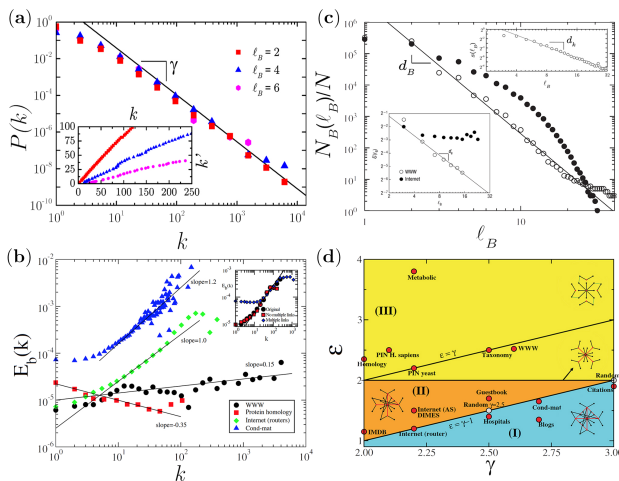


FIG. 1: **Structural self-similarity.** **a)** Scale-invariance of the WWW under the chemical-space RG for different box sizes ℓ_B . (Inset) Scaling of k' versus k in the WWW for different ℓ_B . **b)** Characterization of degree-degree correlations via $E(k)$ (see text). The exponent $\epsilon > 1$ quantifies the network's correlations: $\epsilon_{rand} = \gamma - 1$ for random graphs while $\epsilon_{hier} = \gamma$ for hierarchical scale-free trees [58]. (Inset) Scale-invariance [57] of $E(k)$ for the Internet (router level) under chemical-space RG with $\ell_B = 3$. **c)** Scaling factors related to the network's size N'/N , its largest degree $s(\ell_B) \equiv k'/k$ (upper inset), and its hub-hub correlations $\mathcal{E}(\ell_B) \equiv n_h/k'$ with n_h the number of links connected to hubs (lower inset) versus ℓ_B , under the chemical-space RG. Fractal networks (e.g. the WWW, open circles) show power-law decays with finite dimensions d_B , d_k and d_e ; non-fractal networks (e.g. Internet, filled circles) show an exponential (or faster) decay, i.e. $d_B, d_k \rightarrow \infty$ and $d_e \rightarrow 0$. **d)** Classification of scale-free networks in the (γ, ϵ) -plane [57]. Besides the lines $\epsilon_{rand} = \gamma - 1$ (confining the area I of random models) and $\epsilon_{hier} = \gamma$ defined in **b)**, the scaling relation $\epsilon = 2 + d_e/d_k$ distinguishes non-fractal ($\epsilon \leq 2$, area II) from fractal networks ($\epsilon > 2$, area III).

due to its underlying disassortativity, giving rise to clusters of nodes around isolated hubs. Rooting on this property, Song, Havlin & Makse (SHM) formulated [12, 16] a recursive network model where hub-hub correlations and the degree of modularity can be tuned in a probabilistic way (Fig. 2B)).

Besides introducing a theoretical framework for linking the self-similar behaviors observed in real-world systems to the microscopic growth rates controlling their evolution [58], the SHM model opened a new frontier in the study of complex networks, enabling to analyze the formation of many biological networks and to trace back the evolutionary path of present day structures starting from their original ancestors [68].

RG flow and universality. The repeated application of the chemical-space RG transformation, \mathcal{R}_b , identifies a flow in the space of all the possible graphs which, much like the case of critical phenomena [55, 56], enables a classification of network topologies into *universality classes*. Scale-invariance and self-similarity, in fact, are natural symmetries featured by the fixed points of the RG flow, whose stability against small perturbations enshrines universal features.

A preliminary study aiming at this direction was carried out by Radicchi *et al.* in Ref. [14]. Here, the RG flow of the variable $\kappa_t := k_t^{max}/(N_t - 1)$ – where k_t^{max} and N_t are respectively the largest degree and the size of the renormalized network $G_t = \mathcal{R}_b(G_{t-1}) = \dots = \mathcal{R}_b^t(G_0)$ at the t^{th} RG step (with G_0

the initial network) – and its corresponding fluctuations $\chi_t = N_0(\langle \kappa_t^2 \rangle - \langle \kappa_t \rangle^2)$, were analyzed as functions of the relative network sizes $x_t = N_t/N_0$. Generalizing classical finite-size scaling arguments, the authors of Ref. [14] showed that the observables κ_t, χ_t respectively obey the scaling relations

$$\kappa_t = F(x_t N_0^{1/\nu}), \quad \chi_t = N_0^{\gamma'/\nu} H(x_t N_0^{1/\nu}), \quad (2)$$

where F, H are scaling functions and γ', ν are exponents to be determined. Scrutinizing a large set of real-world and artificial networks [66], a coherent picture emerged: non-fractal networks (e.g., ER graphs, Watts-Strogatz networks, the PA model, etc.) feature the exponents $\nu = \gamma' = 2$ (Fig. 3a), while fractal networks (e.g. the SHM model, Apollonian networks, percolating clusters, etc.) yield values of γ and ν different from 2. In particular, for the SHM model, it was shown [14] that $\nu = \gamma' = 1$ (Fig. 3b) for every value of the SF exponent γ , while $\nu = \gamma' = 2$ after any arbitrarily small random rewiring, suggesting that fractal topologies are *unstable* fixed points of the RG flow. This instability can be intuitively understood in terms of the fragile nature of fractality against structural perturbations. In fact, for increasing fractions of randomly drawn shortcuts, fractal networks rapidly cross over to more and more compact architectures (Fig. 3c,d) having weaker and weaker modularity. This leads to networks featuring the fractal scaling $\bar{\ell} \sim N_0^{1/d_B}$ up to a certain length-scale before the global small-world behavior $\bar{\ell} \sim \ln N_0$ is observed (Fig. 3e).

After this initial step, a second fundamental breakthrough appeared in Ref. [15], where a firm RG flow analysis allowed to elegantly elucidate the universal features of the fractal to small-world transition in complex networks. In this work, Rozenfeld *et al.* showed that adding shortcuts to a fractal network G_0 with probability $p(\ell) = \mathcal{A}\ell^{-\alpha}$, where \mathcal{A} is a normalization constant, brings the RG trajectories either to converge towards G_0 or to transform it into a complete graph – a trivially stable fixed point – depending on the value of the exponent $\alpha > 0$. To quantify these ideas, the authors focused on the renormalized distribution p_b of shortcuts after one RG step which, in the formal limit of $\ell_B \rightarrow \infty$, leads to the fixed point equation [15]

$$p^*(\ell) \equiv 1 - \lim_{x \rightarrow \infty} \exp\left[-C(\ell)x^{2d_B/\alpha-1}\right], \quad (3)$$

where $C(r) \equiv \mathcal{A}^{2d_B/\alpha} r^{-2d_B}$ and $x \equiv \mathcal{A}^{-1}(\ell_B \ell)^\alpha$. Eq. (3) has three distinct solutions (Fig. 3f), depending on the value of the parameter $s \equiv \alpha/d_B$:

- if $s > 2$, then $p^*(\ell) = 0$ and the RG flow converges again towards the fractal network G_0 ;
- if $s < 2$, then $p^*(\ell) = 1$ and the flow converges towards the complete graph K ;
- if $s = 2$, then the RG flow has a non-trivial stable fixed point G' , consisting of G_0 dressed with shortcuts following $p^*(\ell) = 1 - \exp(-\mathcal{A}\ell^{-2d_B})$.

To gain further insights into these three phases, Rozenfeld *et al.* [15] further studied the flow of the difference $z_b - z_0$ between the average degrees in G_0

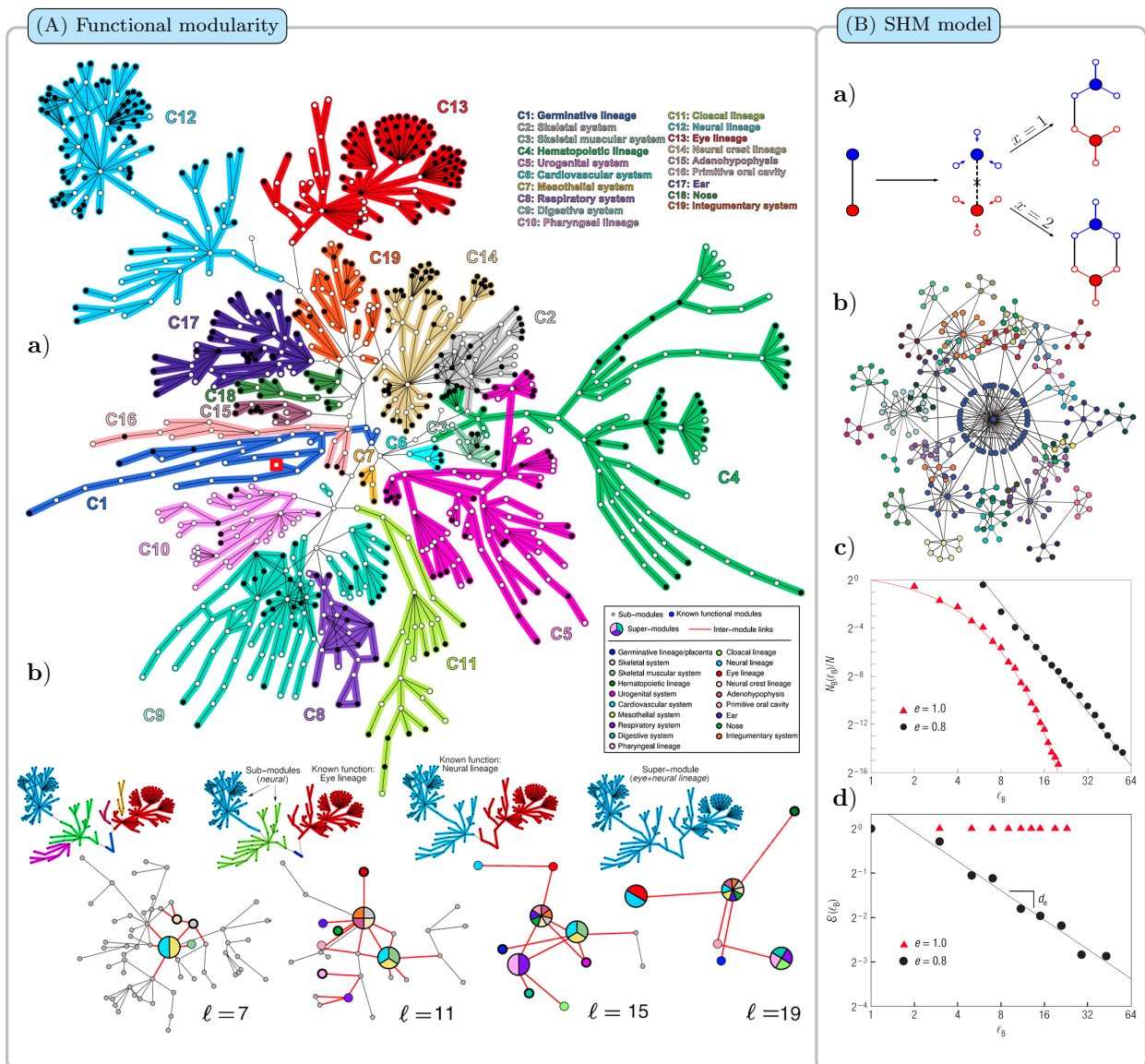


FIG. 2: **A) Functional modularity.** **a)** Network of the human cell differentiation based on cell types (nodes) and differentiation steps (links) from the fertilized egg (red square) to a developed human, modularly colored according to their *known* functions (courtesy of Ref. [63]). **b)** Module detection and RG analysis for two particular functions, identifying a hierarchy of sub-modules (gray dots, in the renormalized network), known functions (colored circles) and super-modules (pie-charts) of size ℓ plotted in different colors. The entire neural (C12) and eye (C13) systems are respectively detected at $\ell = 11$ and $\ell = 15$, while new functional relations emerge at different scales. **B) Evolution: the SHM model** [16]. **a)** At each step and for every link, a node produces m offsprings. The original link is then removed with probability e , and x new links between randomly selected nodes of the new generation are added. Illustration: $m = 3$, $e = 1$. While e tunes between pure fractals ($e = 1$) and pure small-worlds ($e = 0$), x rules the degree of modularity, so that $x = 1$ yields tree-like structures and shortcuts among modules appear for $x > 1$. **b)** Example for $m = 1.5$, $e = 0.5$ and x is 1% of the total number of links at each step, resulting into a scale-free network which is fractal and modular up to a cut-off scale above which it becomes a small-world. **c, d)** For $x = 1$, the model satisfies the fractal scaling in Eq. (1) and the exponential decay expected for small-worlds, as well as the expected correlation patterns (compare with Fig. 1c).

and in the renormalized network $G_b = \mathcal{R}_b(G')$. They found that $z_b - z_0 = (z' - z_0)\mathcal{D}(x_b)$ where, in the thermodynamic limit, the function $\mathcal{D}(x_b)$ scales with the relative network size as $\mathcal{D}(x_b) \sim x_b^\lambda$ and the RG exponent λ depends on the shortcut exponent α as

$$\lambda = \begin{cases} 1, & \text{if } s \leq 1, \\ 2 - s, & \text{if } s > 1. \end{cases} \quad (4)$$

As summarized in Fig. 3g, Eq. (4) identifies two transitions in the space of network configurations: *i)* a small-world to fractal transition at $s = 2$, equivalently at $\alpha = 2d_B$, separating the stable ($\lambda < 0$, $s > 2$) phase of compact topologies from the unstable phase ($\lambda > 0$,

$s < 2$) of modular structures; *ii)* a *navigability transition* at $s = 1$, equivalently at $\alpha = d_B$, identifying the network analogue of Kleinberg's optimal point [69].

Besides raising theoretical questions regarding the characterization of these configurational transitions, the RG theory sketched above provides an indirect method for extracting information about the distribution of shortcuts in fractal real-world networks – a crucial ingredient for understanding information flow and optimal search [70] – and to determine their approximate location in the space of network configurations. The results of an analysis of this kind applied to the WWW, the metabolic network of *E. coli*, a yeast

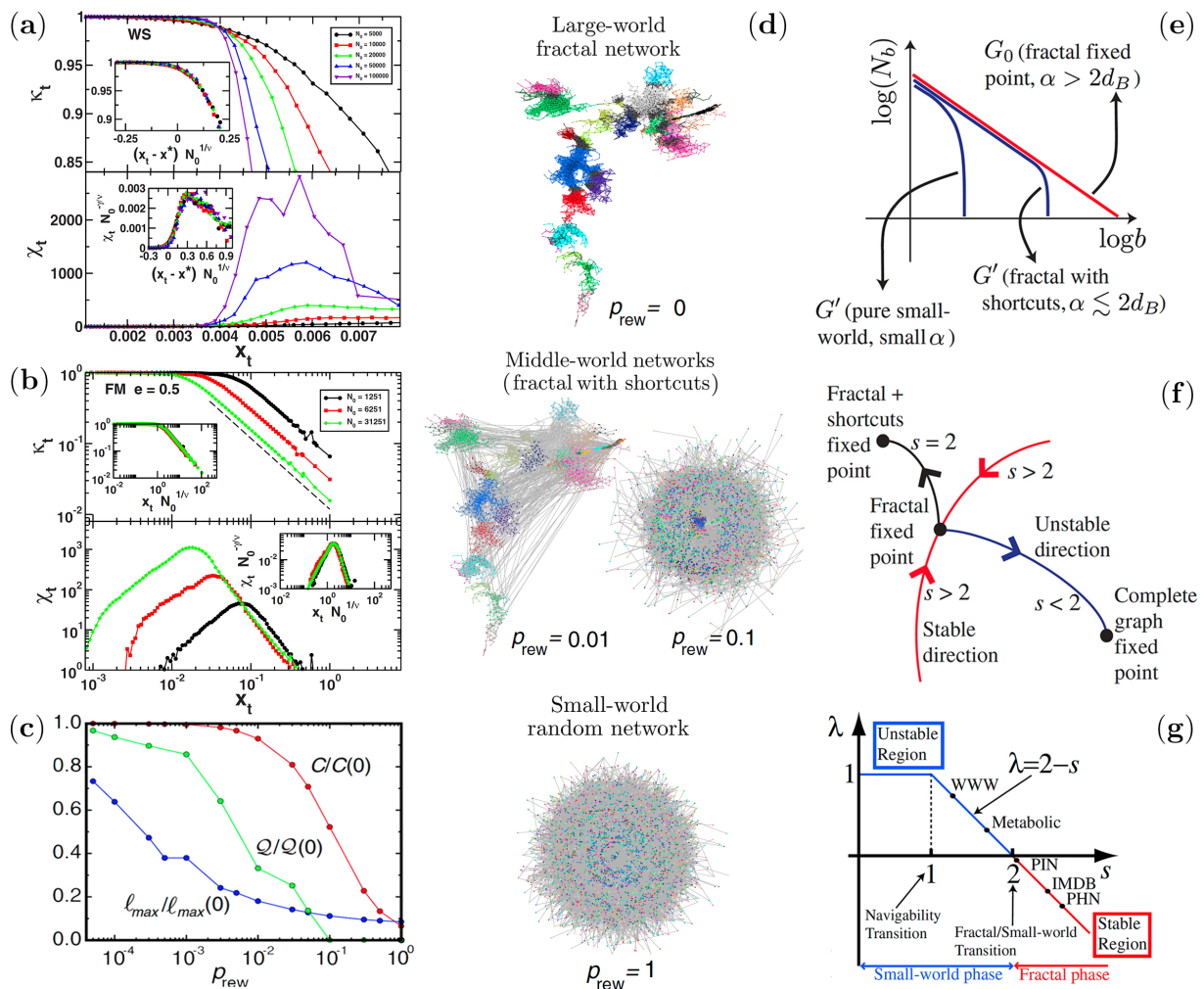


FIG. 3: **Chemical-space RG flow.** **a)** Effects of structural perturbation on the RG flow for a Watts-Strogats (WS) network, with $\langle k \rangle = 4$ and a fraction $p = 0.01$ of shortcuts [14, 66]. Scaling of κ_t (top), χ_t (bottom) versus x_t , and their collapse (inset) according to the scaling relations described in Eq. (2), leading to $\nu = \gamma' = 2$. **b)** Similar analyses performed on a SHM network with $e = 1/2$ yield instead [14, 66] the exponents $\gamma' = \nu = 1$. **c)** Fractal to small-world transition by randomly rewiring a fraction p_{rew} of the total number of links. **d)** Structural variations for the networks in **b)**, measured in terms of the modularity factor \mathcal{Q} , the diameter ℓ_{max} and the clustering C for increasing p_{rew} . While modularity is rapidly lost, small-worldness is rapidly gained, emphasizing the trade-off between these network features (courtesy of Ref. [67]). **e)** Crossover from the power-law scaling in Eq. (1) to an exponential decay in fractal networks upon the addition of shortcuts according to the probability $P(\ell) = A\ell^{-\alpha}$. **f)** RG flow diagram in the space of configurations [15]. In the stable phase ($s \equiv \alpha/d_B > 2$) the RG flows converges to the fractal fixed point, while in the unstable phase ($s < 2$) it flows towards a complete graph. For $s \simeq 2$ the scaling has an exponential cut-off (shown in **d)**) indicating that globally the network is a small-world, while exhibiting fractality at small scales. **g)** Phase diagram and universality. The stability analysis of the RG flow (enshrined in the stability exponent λ) leads to Eqs. (3)–(4), in terms of which a navigability ($s = 1$) and a fractal to small-world ($s = 2$) transitions are identified, leading to a classification of real-world complex networks in the space of network configurations (courtesy of Ref. [15]).

protein interaction network (PIN), the actors network of IMDB, and the protein homology network (PHN), are depicted in Fig. 3g. The results show, in particular, that the WWW is fractal (Fig. 1c) up to a given length scale, but it is also sufficiently randomized for hosting an optimal flow, as manifested by its proximity in the (λ, s) plane to the navigability threshold.

II. HYPERBOLIC GEOMETRY OF LATENT SPACES

A deep connection between self-similarity and fractal properties of the structure of real-world networks, as discussed above, and hyperbolic geometry has been well explored in mathematics [34, 71, 72]. The con-

nection goes via the observation that any Gromov-hyperbolic space has a boundary at infinity which is always a self-similar metric space [72]. Another aspect of this connection is that self-similar groups can be always represented as the groups of automorphisms of trees, which are the simplest example of discrete hyperbolic spaces [71]. The connections between hyperbolicity and self-similar sets, fractals, and similar objects goes also through the idea that rescaling is (approximately) an isometry transformation in (coarse) hyperbolic geometry [73]. Yet this geometry turned out to be not the geometry of the observable structure of real-world networks discussed above, but the geometry of their latent spaces that we discuss next. The two geometries are intimately related because, as we explain below, the shortest paths in networks, defin-

ing chemical distances, follow closely their hyperbolic geodesics in the latent space in most scenarios. Whenever this happens, the network is said to be congruent with its underlying latent geometry.

Models. Latent space approaches have been employed for nearly a century to model homophily in social networks [76–78]. In these models, nodes are positioned in a similarity space, while connections between them are random, but they are the more likely, the closer the two nodes in the space, i.e. more similar nodes are more likely to be connected.

These models are known as (*soft*) *random geometric graphs* in mathematics, where they have been extensively explored [79]. In the simplest random geometric graph model, n nodes are placed uniformly at random on the interval $[0, n]$ with periodic boundary conditions, a circle, and connected if the distance between them is less than parameter $\mu > 0$ controlling the average degree ($\langle k \rangle = 2\mu$). The model yields networks with non-vanishing clustering ($\langle c \rangle = 3/4$) and average shortest path length that scales linearly with network size, that is, the networks are large-worlds, as a reflection of the metric structure of the space.

From the statistical physics perspective, this model is the zero-temperature limit of a more general entropy-maximizing probabilistic mixture of grand canonical ensembles with the Fermi-Dirac probability of connection between nodes i and j :

$$p_{ij} = \frac{1}{e^{\beta(\varepsilon_{ij}-\mu)} + 1}. \quad (5)$$

In this ensemble, edges are fermions with energies

$$\varepsilon_{ij} = f(x_{ij}), \quad (6)$$

where $f(x_{ij})$ can be any non-decreasing function of distances between nodes on the circle, β is the inverse of the temperature fixing the average energy of the networks, and μ the chemical potential controlling the expected number of particles-edges. A choice of $f(x)$ defines network properties in the ensemble. However, only if $f(x) \propto \ln x$ and $\beta \in (1, 2)$, the networks are sparse small worlds and have non-vanishing clustering at the same time [80].

The distribution of node degrees in such models is homogeneous, but it can be modified to yield any degree distribution—in particular, power-law distributions ubiquitous in real-world networks. This modification sets the edge energy given in Eq. (6) to

$$\varepsilon_{ij} = \ln \frac{x_{ij}}{\kappa_i \kappa_j}, \quad (7)$$

and hence the connection probability in Eq. (5) to

$$p_{ij} = \frac{1}{1 + \chi_{ij}^\beta} = \frac{1}{1 + \left(\frac{d_{ij}}{\mu \kappa_i \kappa_j}\right)^\beta}, \quad (8)$$

where κ_i is the expected degree of node $i = 1, \dots, n$ in the ensemble [81], known as the \mathbb{S}^1 model (Fig. 4a). The values of parameters κ_i can be either fixed or random, sampled from any desired distribution. If, e.g., they are sampled from the Pareto distribution $\rho(\kappa) = (\gamma - 1)\kappa_0^{\gamma-1}\kappa^{-\gamma}$, the resulting degree distribution is

Pareto-mixed Poisson, which is asymptotically a power-law $P(k) \sim k^{-\gamma}$ for $k \gg 1$ [82]. The definition of edge energy in Eq. (7) combines the popularity (degrees κ_i) and similarity (distances x_{ij}) dimensions into a single measure, while the connection probability takes the gravity law form in Eq. (8) decreasing with the similarity distance x_{ij} and increasing with the popularity product $\kappa_i \kappa_j$. Notice that introducing degree heterogeneity preserves the maximum-entropy property, so that the \mathbb{S}^1 model is the only entropy maximizing ensemble that can produce sparse heterogeneous networks with the small world property, nonzero clustering, and no degree correlations [80].

If $\beta > 1$ and $\rho(\kappa)$ is Pareto, the map $\kappa \mapsto y = \kappa^2$ places all nodes i at coordinates (x_i, y_i) , $x_i \in \mathbb{R}$, $y_i > \kappa_0^2$, in the upper half-plane model of the hyperbolic plane \mathbb{H}^2 [83]. If $\gamma = 3$, then nodes are distributed uniformly there according to the hyperbolic metric $ds^2 = (dx^2 + dy^2)/y^2$. The group of distance-preserving isometries of the half-plane is isomorphic to the Lorentz group $SO(1, 2)$. The Lorentz boosts, i.e., hyperbolic rotations in the 3-dimensional Minkowski space, act on the upper half-plane as space-rescaling transformations $x \mapsto x' = \xi x$, $y \mapsto y' = \xi y$, where $\xi > 0$ [84]. The energies

$$\varepsilon_{ij} = \ln \frac{x_{ij}}{\kappa_i \kappa_j} = \ln \frac{x_{ij}}{\sqrt{y_i y_j}} \quad (9)$$

are thus manifestly invariant, and so is the model, with respect to rescaling Lorentz boosts, which form a non-compact subgroup of all isometries of the hyperbolic plane. However, the model is not invariant with respect to all isometries of the full Lorentz group since energy is not exactly a function of the hyperbolic distance, and so neither is the connection probability. This problem is fixed in a slightly different but asymptotically equivalent model [18] defined by the map $\kappa \mapsto r = R - 2 \ln \kappa$, $R = 2 \ln(n/\nu)$, ν the parameter controlling the average degree. This map places nodes i at polar coordinates (r_i, θ_i) , $\theta_i = 2\pi x_i/n$, on the hyperbolic disc of radius R in the hyperboloid model of the hyperbolic plane with metric [83] $ds^2 = dr^2 + \sinh^2 r d\theta^2$ [83] (Fig 4b). The edge energy becomes

$$\varepsilon_{ij} = \frac{1}{2} \left(r_i + r_j + 2 \ln \frac{\theta_{ij}}{2} \right) \approx \frac{1}{2} d_{ij}, \quad (10)$$

where θ_{ij} and d_{ij} are the angular and hyperbolic distances between the two nodes [188] so that the connection probability reads

$$p_{ij} = \frac{1}{1 + e^{\frac{\beta}{2}(d_{ij}-R)}}. \quad (11)$$

If $\gamma = 3$ and $\beta \rightarrow \infty$, the model has the simplest formulation: sprinkle n points uniformly at random over a hyperbolic disc of radius R , and then connect all pairs of points located at distance $d_{ij} < R$ from each other, Fig. 4b shows the equivalence between the \mathbb{S}^1 model and this \mathbb{H}^2 representation. Since energy is a function of the distance Eq. (10), the model is fully Lorentz-invariant in the $n \rightarrow \infty$ limit for any β .

The two quasi-isomorphic models defined by Eqs. (7) and (10) generalize to spheres \mathbb{S}^D of any dimension D ,

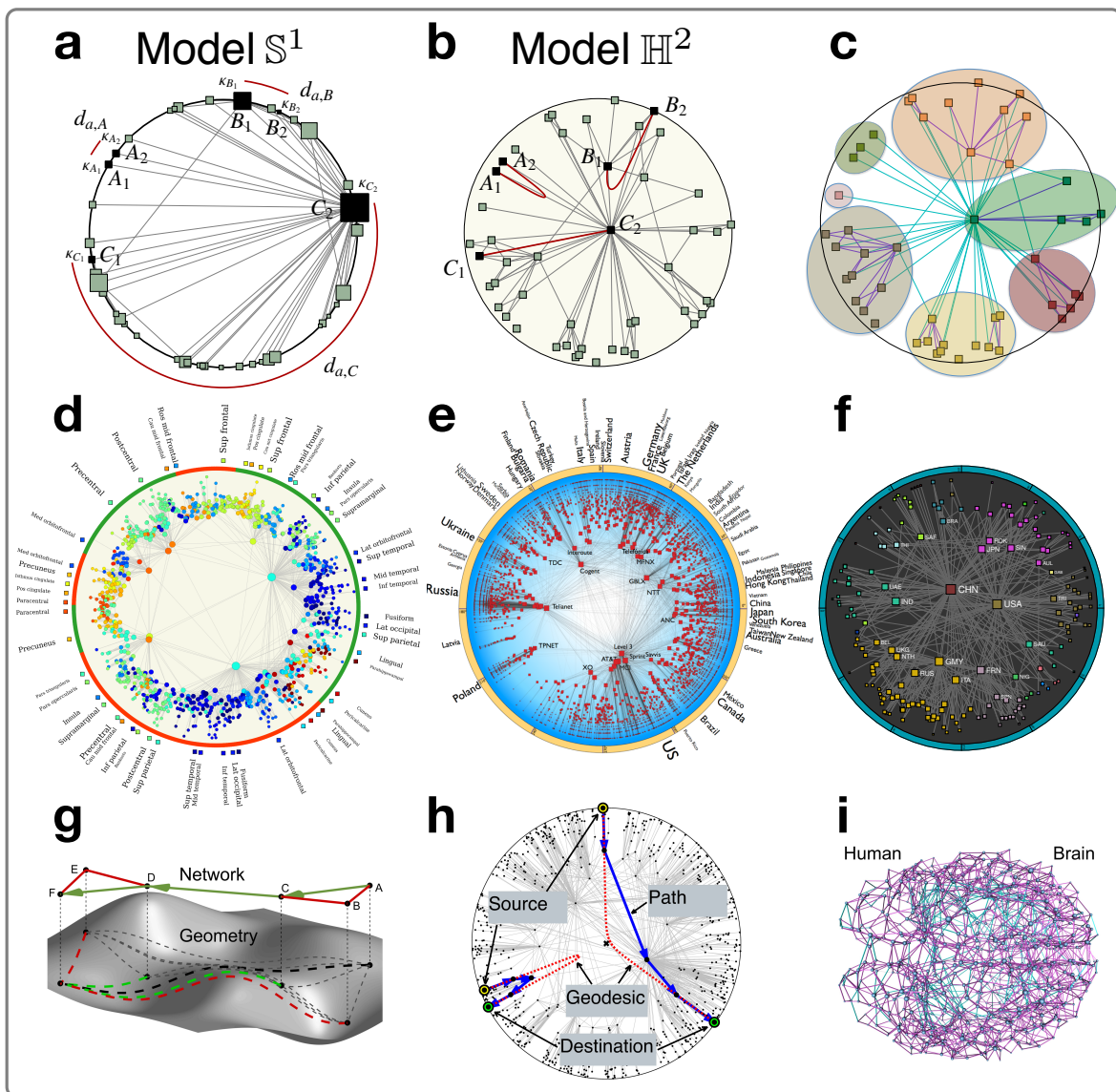


FIG. 4: **Networks in latent geometry.** **a–c) Models.** **a)** Model \mathbb{S}^1 . The similarity distances d_a between pairs of nodes A_1 - A_2 , B_1 - B_2 and C_1 - C_2 have been highlighted. The size of a node is proportional to its hidden degree κ . **b)** Model \mathbb{H}^2 in the hyperbolic plane. Nodes in the different pairs are separated by the same hyperbolic distance. Nodes are equally sized but nodes with higher hidden degree are positioned closer to the centre. The similarity distance is the same in the two representations. **c)** Sketch illustrating the Critical Gap Method (CGM). Nodes are partitioned into different groups separated by void angular gaps. The modularity of the partition is computed by comparing the number of links within the communities (purple links) to the number of links between nodes in different communities (green links). The partition with the highest modularity is eventually selected. **d–f) Embeddings of real networks and their community organization.** **d)** Human brain connectome [74]. Different node colors correspond to different anatomical brain regions. **e)** Internet at the Autonomous Systems level [75]: The name of each country is located at the average angular position of its Autonomous Systems. **f)** World trade map in 2013 [23]: Different node colors correspond to different communities detected by the CGM method. **g–i) Geometric routing.** **g)** Finding a path from A to F in the network is done step-by-step. The source node A first checks which one of its neighbors in the network, B or C , is closer to the destination node F in the underlying geometry, where the geodesics are shown by the dashed curves. Node C is closer, so that it is the next hop on the path from A to F . Node C then performs similar calculations to find that D is closest to F among its network neighbors A, B, D , so that D is the next hop after C , and also a penultimate hop because it is a neighbor of F . **h)** Proximity of shortest paths in hyperbolic networks to hyperbolic geodesics. The blue arrows show the paths that geometric routing finds between a couple of source-destination pairs in a hyperbolic network. The found paths are also the shortest paths in the network in terms of the number of hops. The hyperbolic geodesics between the corresponding sources and destinations in the hyperbolic plane are shown as the dashed red curves. **i)** Navigation skeleton of the human brain [20]. The structural network of the human brain with links colored depending on whether they belong (magenta) or do not belong (cyan) to the minimal network that enables maximal navigability in the brain.

and to hyperbolic spaces \mathbb{H}^{1+D} , with edge energy $\epsilon_{ij} = \ln \frac{x_{ij}}{(\kappa_i \kappa_j)^{1/D}} \approx d_{ij}/2$ [81]. The equivalence between the two models is a reflection of the isomorphisms between the Lorentz group $SO(1, D+1)$ and the Möbius group acting on sphere \mathbb{S}^D as the group of its conformal transformations. This isomorphism is a

starting point of the anti-de Sitter/conformal field theory (AdS/CFT) correspondence in string theory [85]. The models have been also adapted to growing networks [25], in which case the latent space is not hyperbolic but de Sitter space $d\mathbb{S}^{1,D}$ with the same Lorentz group $SO(1, D+1)$ of symmetries [86], as well as to

weighted networks [87], multilayer networks [88, 89], and to networks with community structure [21, 22, 90]. At present, this is the only class of models that captures sparsity, the small-world property, power-law degree distributions, nonvanishing clustering, and community structure, in a purely geometric framework with explicit symmetry structure.

Maps of real networks. A collection of methods have been developed for inferring the latent coordinates of nodes in a given network using techniques from statistical inference and machine learning [75, 91–99]. The application of these methods to real-world networks (Fig. 4d–f) revealed the existence of geometric communities [23, 100], and helped to decode mechanisms that govern network evolution, such as globalization, localization, and hierarchization driving the evolution of international trade [23]. At the same time, maps of real networks boost the understanding of many dynamical processes, including cooperation in social networks more strongly controlled by the latent-space organization than by highly-connected hubs in the system [101]. One of the most practical applications of mapping real-world networks to their latent geometries is the design of efficient and scalable routing protocols for the Internet [75] and for emerging Internet-of-Things telecommunication networks [102]. Finally, embeddings of real networks allow their investigation at different resolutions by application of a geometric renormalization group that unfolds the networks in a self-similar multilayer shell that distinguishes the coexisting scales and their interactions [48].

Geometric communities. The angular distribution of nodes in the geometric network models \mathbb{S}^1 and \mathbb{H}^2 is uniform. However, nodes in maps of real networks concentrate in specific regions defining geometric communities in many systems, including the Internet [75], metabolic networks in cells [100], trade networks [23], and brain connectomes [103]. Non-overlapping communities can be detected in the geometric domain using purely geometric methods. One definition considers soft communities as groups of nodes in similarity space separated from the rest by angular gaps that exceed a certain critical value [100]. An alternative, known as the Critical Gap Method (CGM) [23], finds the communities by changing the gap and selecting the soft community partition that maximizes the standard modularity measure [64], Fig. 4 c,f. These distance-based communities show strong correlation with groups defined by metadata, like geographical location of the Autonomous Systems in the case of the Internet, biochemical pathways of reactions in metabolic networks, or anatomical brain region in structural brain networks [104], Fig. 4 d,e.

Navigability. One of the main strengths of the discussed latent-geometric network models lies in an explanation of the efficiency of this structure with respect to one of their most common functions, which is transport of information, energy, or other media, without the global knowledge of the network structure [19]. Latent space guides navigation in the network based on distances between nodes in the space [19]. That is, instead of finding shortest paths in the network – a computationally intensive combinatorial problem in a

dynamic network [105] – a transport process can be geometric, relying only on geodesic distances in the space (Fig. 4 h). Such processes are the more efficient and robust, so that the network is the more navigable, the smaller the γ , and the larger the β , defining a navigable parameter range to which many real-world networks belong [19]. Networks in the hyperbolic model described above are nearly maximally efficient for such geometric navigation [18], which has recently been proven rigorously [106]. The main reason behind this phenomenon is the proximity of shortest paths in hyperbolic networks to the corresponding geodesics in the underlying hyperbolic geometry (Fig. 4 h). Another critical factor is the existence of superhubs interconnecting all parts of the network, present as soon as $\gamma < 3$ [18], in which case the networks are known to be ultrasmall worlds [52]. It was demonstrated in Ref. [107] that navigation in hyperbolic networks with $\gamma < 3$ can always find these ultrashort paths, and thus navigation in these networks is asymptotically optimal. The other way around, networks that are maximally navigable by design turned out to be similar to hyperbolic networks, and many real-world networks were found to contain large fractions of their maximum-navigability skeletons [20], the human brain example shown in Fig. 4 j. Assuming that real-world networks evolve to have a structure efficient for their functions, these findings provide an evolutionary perspective on the emergence of latent geometry leading to structural commonalities observed in many different real-world networks.

Renormalization and self-similarity. Since networks in the discussed models are purely scale-invariant in the thermodynamic limit, they contain an infinite hierarchy of self-similar nested subgraphs induced by nodes with degrees exceeding a given threshold, as illustrated in Box B. This observation also applies to many real networks, where the average degree of the subgraphs increases as a function of the degree threshold [81]. This property allows to prove easily the absence of percolation or epidemic thresholds in these networks, independently of the commonly used tree-like or scale-free assumptions. The proof is general and is solely based on a symmetry principle. Thus, it also applies to any phase transition whose critical point is a monotonic function of the average degree [108], like in SIS type epidemic spreading or in the Ising model, that in scale-free networks lack a healthy phase [109] or a disordered phase [110], respectively.

Self-similarity is also observed in the multiscale organization of networks, that can be explored at different resolutions by applying a geometric renormalization transformation [48] inspired by concepts from the renormalization group in statistical physics [55, 111]. The method relies on similarity distances to coarse-grain neighboring nodes into supernodes defining a new rescaled map, see Box C. The iteration of the transformation unfolds a network into a multiscale shell that progressively selects longer range connections revealing the coexisting scales and their interactions. Self-similarity under geometric renormalization is an ubiquitous symmetry in real-world networks, in good agreement with the prediction given by the renormalizability of the underlying \mathbb{S}^1 model [48], Fig. 5.

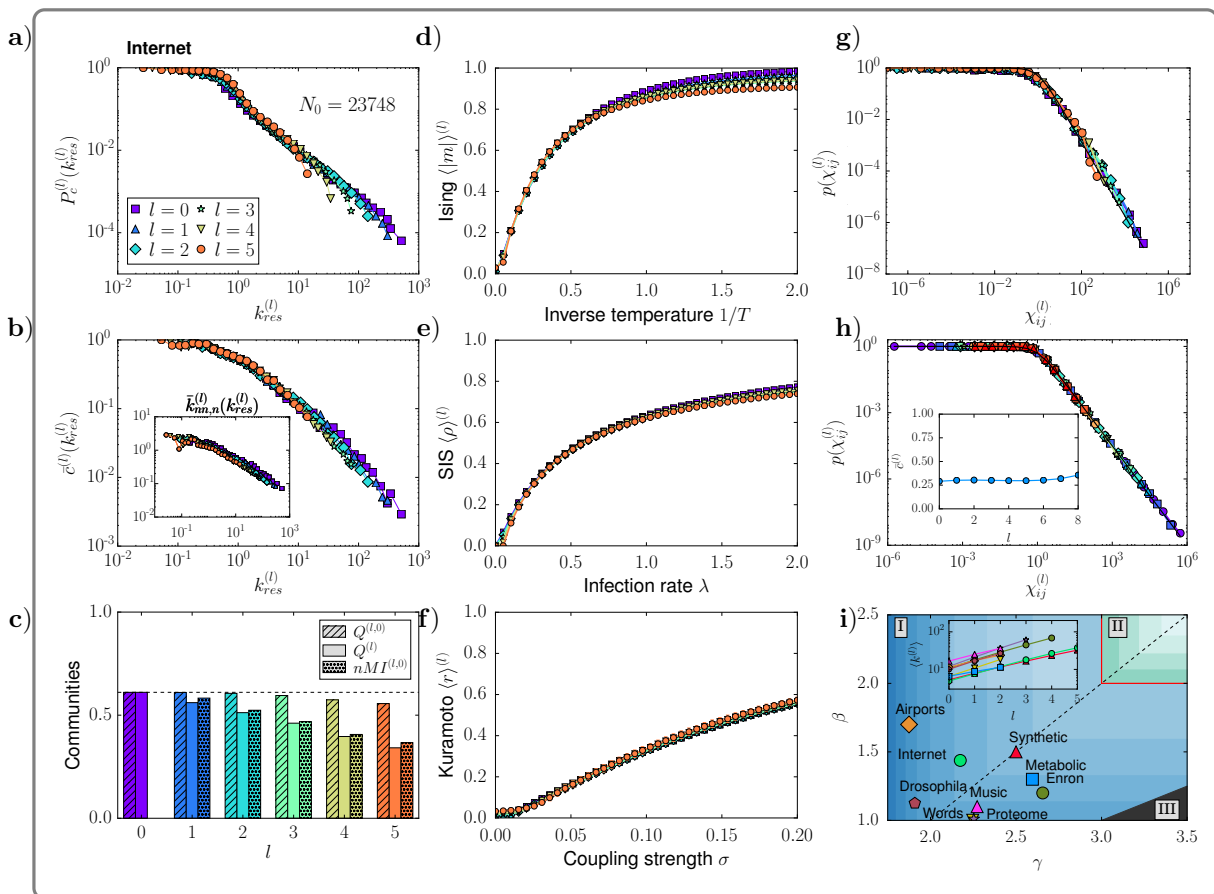


FIG. 5: **Multiscale unfolding of networks' structure and function by geometric renormalization.** Self-similarity of the structural and dynamical properties of the multiscale 5-layered geometric renormalization shell of the Internet (a–g), and renormalizability of the \mathbb{S}^1 model (h–i) (courtesy of Ref. [48]). **a)** Degree distribution. **b)** Clustering spectrum. Inset: average nearest neighbors degree. **c)** Topological community structure. **d–f)** Simulation of the Ising dynamics, SIS epidemic spreading dynamics and Kuramoto model for synchronization in the different layers of the shell. Results averaged over 100 simulations. **d)** Magnetization $\langle |m| \rangle^{(l)}$ of the Ising model as a function of the inverse temperature $1/T$. **e)** Prevalence $\langle \rho \rangle^{(l)}$ of the SIS model as a function of the infection rate λ . **f)** Coherence $\langle r \rangle^{(l)}$ of the Kuramoto model as a function of the coupling strength σ . **g)** Empirical connection probability in the Internet and the renormalized layers measured as the fraction of connected pairs of nodes as a function of $\chi_{ij}^{(l)} = R^{(l)} \Delta \theta_{ij}^{(l)} / (\mu^{(l)} \kappa_i^{(l)} \kappa_j^{(l)})$. **h)** The same as in **g)**, now for a synthetic \mathbb{S}^1 network with $N \approx 225000$ nodes, $\gamma = 2.5$ and $\beta = 1.5$. The black dashed line shows the theoretic curve given in Eq. (8). Inset: invariance of the mean local clustering along the flow. **i)** Real networks in the connectivity phase diagram of the \mathbb{S}^1 renormalization flow. The synthetic network above is also shown. Darker blue (green) in the shaded areas represent higher values of the exponent ν controlling the flow for the average degree $\langle k \rangle^{(l+1)} = r^\nu \langle k \rangle^{(l)}$. The dashed line separates the γ -dominated region from the β -dominated region. In phase I, $\nu > 0$ and the network flows towards a fully connected graph. In phase II, $\nu < 0$ and the network flows towards a one-dimensional ring. The red thick line $\nu = 0$ indicates the transition between the small-world and non-small-world phases. In region III, the degree distribution loses its scale-freeness along the flow. The inset shows the exponential increase of the average degree of the renormalized real networks $\langle k(l) \rangle$ with respect to l .

This result suggests that the same connectivity law rules short and long range connections and operates at different length scales. From a practical point of view, applications include scaled-down network replicas and a multiscale navigation protocol that takes advantage of the increased navigation efficiency at higher scales. Interestingly, the structure of the human brain remains self-similar when the resolution length is progressively decreased by hierarchical coarse-graining of the anatomical regions, a symmetry that is well predicted by the geometric renormalization [103].

III. GEOMETRY OF NETWORK-DRIVEN PROCESSES

Evidence for the existence of self-similarity and fractal properties characterizing the topology of empirical

networks provided a solid ground for exploring the latent geometry of their structure in the hyperbolic space. The existence of a hidden geometry of network structure naturally led to question if a hidden geometry of network dynamics – aiming at identifying the latent space due to system function arising from the interplay between structure and dynamics – was plausible. Note that network dynamics is broadly defined, including the dynamics of vertex and edge creation or destruction – including, for instance, system's growth over time or time-varying topology – as well as the dynamics of processes on the network. The hidden geometry induced by dynamics has been mostly explored for the latter, with geometric tools have found fertile grounds also for unraveling hidden patterns lurking the complex behaviors of diverse network-driven processes. However, since it is possible to define multiple

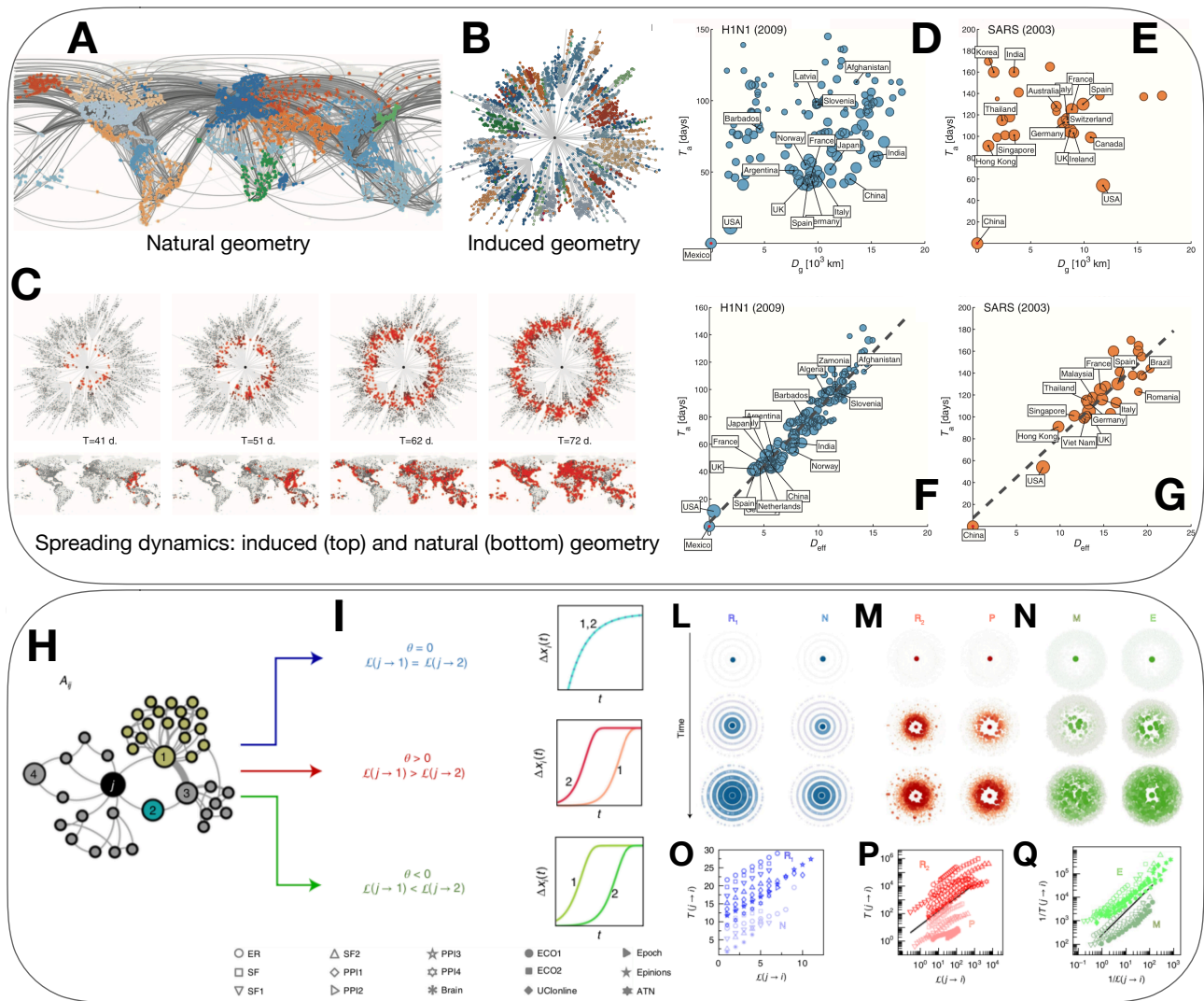


FIG. 6: (Top panel) **Geometry induced by spreading dynamics.** (A) Network representation of passenger flows along direct connections (edges) among airports (nodes) worldwide, with node color encoding geographic regions according to modularity maximization. The natural geometry of the network is given by its embedding into the physical space, with geodesic distance D_g . (B) The same nodes are embedded into a latent geometric space defined by effective distance D_{eff} (see the text for details) accounting for the spreading dynamics on the top of the network. The center of this space is a node of the system, usually the one where the spreading originates from. (C) Evolution of a simulated disease spreading originating in Hong Kong (HKG): red symbols encode the prevalence. The top panels sketch the evolution in the latent, whereas the bottom panel shows the same dynamics in the natural space. When the spreading dynamics is depicted by exploiting the induced geometry, complex spatial patterns are mapped to homogeneous wave fronts propagating at constant effective speed. The relation between epidemic arrival times (T_a) and the two distances is shown for two real case studies, namely the spreading of H1N1 (D–F) and SARS (E–G). The relation is nonlinear when geographic distance is used (D–E) whereas it is nicely reproduced by a straight line when effective distance is considered. Reproduced with permission from Ref. [30]. (Bottom panel) **Geometry induced by universal temporal distance.** (H) A signal travels from vertex j to the rest of the system exhibits different spreading patterns, captured by the universal temporal distance $\mathcal{L}(j \rightarrow i)$, (I) impacting different nodes (e.g., 1 and 2) in different ways depending on the type of dynamics (distance-limited, i.e. $\theta = 0$; degree-limited, i.e. $\theta > 0$; composite, i.e. $\theta < 0$). (L–N) The homogeneous propagation of concentric wave fronts emerge from the analysis of a broad spectrum of synthetic and empirical systems. (O–Q) Propagation times $T(j \rightarrow i)$ of real-world signals are in agreement with the temporal distances $\mathcal{L}(j \rightarrow i)$. Reproduced with permission from Ref. [33]

different dynamical processes on the network – e.g., epidemics spreading (see Fig. 6) or random searches (see Fig. 7), one expects not to find a unique latent geometry for system’s function: in principle, there could be as many hidden geometries as the number of plausible network-driven processes. In this universe of dynamical processes, the dynamics of information exchange has been successfully exploited to define novel metric or quasi-metric measures to this aim, the difference being that, in the latter, the symmetry axiom is relaxed.

Remarkably, this class of network geometries provides results about a system’s function that can not be obtained by geometric approaches discussed in the previous sections. An emblematic example concerns the mesoscale organization of interconnected components which exchange information during collective phenomena – e.g., coupled oscillators trying to synchronize or people with social relationships attempting to reach consensus – which can be characterized by mapping the interplay between structure and function to a geometric space induced by diffusion dynamics [112]. The

resulting functional modules differ from the ones obtained by other geometric techniques such as functional modularity maximization [63] (see Fig 2A), since the latter finds an optimal partition of the system while minimizing the possible number of modules of given topological size ℓ , which in turns defines the characteristic distance between nodes within modules. Conversely, modules identified on the diffusion manifold at time τ , determining the scale of dynamics, are characterized by groups of nodes which easily exchange information – e.g., in terms of random searches – within Markov time τ , as we will see in the following.

Geometry induced by communicability. One of the first metrics based on dynamics is the communicability distance [113]. The communicability between two nodes i and j of a network is defined as $G_{ij} = \exp(\mathbf{A})_{ij}$, where \mathbf{A} is the underlying adjacency matrix. From a mathematical point of view, communicability quantifies how well a pair of nodes exchanges information by all possible walks between them, giving more weights to the shortest ones: this can be straightforwardly shown by considering the Taylor expansion of the communicability matrix \mathbf{G} . Communicability is also understood from a physical perspective, if one considers a network where nodes are quantum harmonic oscillators and links are springs, and the system is submerged into a thermal bath with inverse temperature $\beta = 1/kT$, being k the Boltzmann constant. Then communicability provides a representation for the thermal Green's function of the system, indicating how a thermal oscillation propagates between nodes (we refer to Ref. [114] for a thorough review of the physics of communicability in complex networks). The difference between the absorbed and transmitted excitation between two nodes due to such thermal disturbances is quantified by the *communicability distance* [113]

$$\xi_{pq}(\beta) = G_{pp}(\beta) + G_{qq}(\beta) - 2G_{pq}(\beta) \quad (12)$$

allowing to build an hyperspherical embedding of a complex network at different temperatures, representing a geometry which is able to capture, for instance, traffic flows in cities [115] and constrained diffusion in coupled networks [116] such as multilayer systems [117].

Geometry induced by reaction-diffusion. Similarly, it has been shown that a quasi-metric known as *effective distance* can be used to gain insights about reaction-diffusion processes such as the spreading of infectious diseases through mobility networks [30, 118]. Given a network of geographic areas (e.g., airports) and edges encoding direct air traffic – in units of passengers per day – from node i to node j , let F_{ji} indicate the corresponding mobility flow. Let $P_{ij} = F_{ij} / \sum_i F_{ij}$ quantify the fraction of this flow originating from node j directed towards node i , defining the components of the connectivity matrix \mathbf{P} . Despite the structural complexity of the network, involving multiple and often redundant pathways for the transmission of contagion phenomena, the effective distance defined by

$$\delta_{ij} = 1 - \log P_{ij}, \quad (13)$$

reveals hidden pattern geometry where the dynamics of epidemics spreading is elegantly mapped into

the propagation of wavefronts with an effective speed. This latent geometry induced by the dynamics can be used to better predict the arrival times of empirical contagion processes in distinct geographic areas and to reconstruct, with reasonable accuracy, the origin of outbreaks (see Fig. 6).

Similarly, the general dynamics of different signal propagation can be mapped to a *universal temporal distance* defined by

$$\mathcal{L}(j \rightarrow i) = \min_{\Pi(j \rightarrow i)} \left\{ \sum_{p \in \Pi(j \rightarrow i), p \neq j} S_p^\theta \right\}, \quad (14)$$

a metric predictive of actual propagation times $T(j \rightarrow i)$ (see Fig. 6). Here, $\Pi(j \rightarrow i) = j \rightarrow q \rightarrow \dots \rightarrow i$ indicates the shortest path from the origin j to the destination i , while the delay τ_p in signal propagation occurring on each node (p) of this path is assumed to scale as $\tau_p \sim S_p^\theta$, being $S_p = \sum_{k=1}^N A_{ik}$ the weighted degree of the node and $\theta = -2 - \Gamma(0)$ a parameter determined by the system's dynamics [33].

In the same spirit, spreading processes on noisy geometric networks has been recently investigated to understand how contagion dynamics is driven by the underlying topology [31]. Noisy geometric networks provide a suitable framework to model systems characterized by both geometric – i.e., large-world – and non-geometric – i.e., small-world – connections among nodes. Contagion maps, whose manifold structure reflects the interplay between local and non-local structure with the epidemic spreading process, provide a suitable tool to recover the geometric features of a network's underlying manifold and describe wavefront propagation in the corresponding geometric space. This geometric framework allows to gain physical insights on contagions – as well as on other complex dynamics on networked systems – by exploiting computational topology and to identify low-dimensional structure in complex networks [31].

Geometry induced by random search. More recently, random walk dynamics has been proposed to define *diffusion distance* between pair of nodes. Let $\mathcal{L} = \mathbf{I} - \mathbf{T}$ indicate the normalized Laplacian matrix, with I_{ij} the Kronecker delta and T_{ij} the probability for the random walker to move from node i to node j . Let $\mathbf{e}_i \equiv (0, 0, \dots, 1, \dots, 0)$ be the i -th canonical vector in the Euclidean space with dimension N , the size of the system. The evolution over time τ of the probability to find the walker in any node is described by a master equation [119], whose solution is given by $\mathbf{p}(\tau|i) = \mathbf{e}_i \exp(-\tau\mathcal{L})$ when the initial condition is $\mathbf{p}(0) = \mathbf{e}_i$, i.e., the walk's origin is in node i with probability 1. The hidden geometric space induced by Markov dynamics [32] is characterized by the diffusion distance between nodes i and j , defined by

$$d_{i,j}^2(\tau) = [\mathbf{p}(\tau|i) - \mathbf{p}(\tau|j)]^2, \quad (15)$$

providing, among others, the starting point to build diffusion maps which are widely adopted for low-dimensional embedding of high-dimensional data [29]. Two nodes are close in their latent diffusion space if connected by multiple pathways which facilitate information exchange in less than τ steps. As a direct

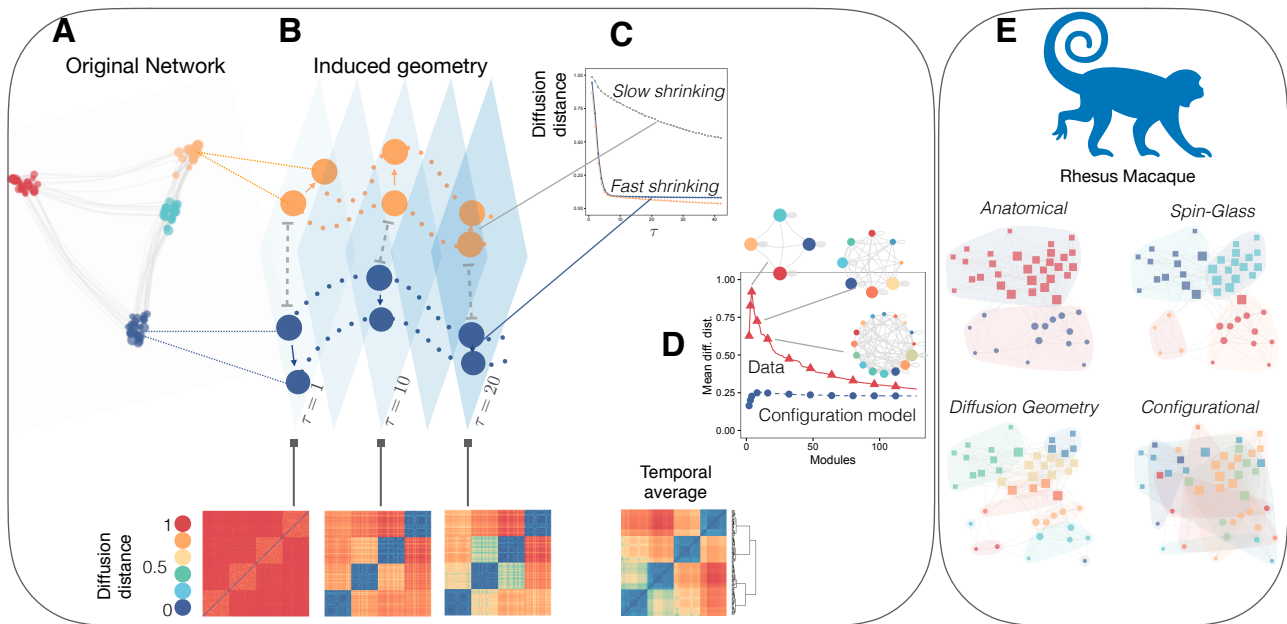


FIG. 7: **Diffusion geometry of complex networks.** (A) Euclidean embedding of a network with four clusters, corresponding to the latent diffusion geometry with $\tau = 1$. (B–C) In the diffusion space, two nodes from the same functional cluster are – and keep – closer across time (τ) than nodes belonging to different clusters. Diffusion-distance matrices corresponding to different Markov times are shown in the bottom and allow to identify the underlying functional organization at different scales. (D) The functional modules maximizing the average diffusion distance define the mesoscale structure which favors the overall information exchange and the significance of this structure can be quantified by comparing against the result obtained from a configuration model preserving the degree distribution of the original data while destroying other correlations. (E) Diffusion geometry analysis of the anatomical connectivity (335 visual, 85 sensorimotor and 43 heteromodal) from 30 visual cortical areas and 15 sensorimotor areas in the Macaque monkey. Clusters identified by structural analysis of the connectome using the spin-glass approach are different, as the anatomical organization and the mesoscale organization obtained from the configuration model. Reproduced with permission from Ref. [32]

consequence, the mesoscale functional organization of the network is mapped into spatial clusters in the corresponding diffusion manifold, with Markov time playing the role of a multi-resolution parameter. Functional hierarchies can be identified at multiple resolutions, with micro-, meso- and large-scale captured for small, increasing and large τ , respectively. The persistence of the average distance between functional clusters across time identifies the mesoscale structure which favors the overall information exchange, providing the best coarse-graining of the system in functional modules (Fig. 7). Geometry induced by diffusive processes allows to gain physical insights about collective phenomena in structured populations, by establishing a formal relationship with complex dynamics responsible for synchronization in the metastable state and emergence of consensus.

The recent application to anatomical connectivity within and between visual cortical and sensorimotor areas in Macaque brain reveals a hierarchical functional organization of cortical units, not identified by existing methods and not compatible with null models [32]. The network embedding in a geometric space allows, and specifically in the one induced by diffusion distance, together with statistical data depth allows for the statistical and most natural generalization of the concept of median to the realm of complex networks, with the advantages for defining the centre of the system and percentiles around that centre to identify vertices which are socially or biologically relevant [120].

IV. DISCUSSION AND OUTLOOK

Endowing complex networks with the notion of distance provided tools and methods complementary to those inspired by classical statistical mechanics, paving the way for their geometrical characterization. Despite its recent inception, network geometry has already served as a remarkably successful pathway to harness the hidden forms and symmetries underlying many real-world systems, leading to a wealth of discoveries of both theoretical and practical importance. The selection of milestones presented in §§ I–III offer a mature viewpoint from where to ponder on some emerging research directions and challenges lying ahead.

From the fractal geometric perspective, the discovery of network’s self-similarity has introduced a spectrum of scaling exponents useful for addressing many longstanding problems, from transport, to the evolution and universality of complex media. While reviewing these results in § I, we purposely omitted discussing about a remarkable feature of networks emerging from the fractal analysis: while both fractal *and* non-fractal structures are self-similar under chemical-space RG (see, e.g. Ref. [16], Fig. S6 and discussions therein), only the former family allows a set of well-defined fractal dimensions, i.e. fractality and self-similarity appear as distinct features under the lens of the chemical distance [121]. The divergence of e.g. the box-counting dimension d_B observed in small-world networks (Fig. 1c) reflects, in some sense, an “ultraviolet” limit above which the

fractal geometric approach fails in quantifying their self-similar symmetry, constraining our understanding only to a partial scenery of a much broader portrait. The identification of a suitable embedding (hence, of an appropriate metric) for curing the divergence of d_B represents a fundamental open challenge, in which respect the hyperbolic geometric approach could be a prominent candidate. While achieving this goal will pave the way at developing a unified framework to e.g. the problem of transport [122] or lead to an exhaustive characterization of RG-based universality classes of complex media, it will further raise exciting perspectives on a more fundamental level. In combinatorics, in fact, the notions of fractal dimensions and self-similarity are intimately related to *ergodic theory* [123], as fractal dimensions can be obtained as ergodic averages in appropriate measure preserving systems [124]. This deep connection reflects into an explicit dependence of the fractal dimension of a given system to the growth rates underlying the RG-maps magnifying it at different length scales. A result pointing in the same direction was reported in Ref. [16], where the growth rates of the SHM model (Fig. 2B) were proved to define the fractal dimensions d_B, d_k, \dots of the generated networks. Extending these results to e.g. the geometric branching growth [27] or to more general growth processes, could yield fundamental insights about the dynamical properties underlying self-similar network evolution.

As far latent hyperbolicity is concerned, it impacted areas as diverse as mathematics, neuroscience, and machine learning. Random graphs have a long research history in graph theory, probability, and adjacent areas in applied mathematics and theoretical computer science (TCS). Given that hyperbolic networks turned out to be the first popular ensemble of random graphs reproducing not only inhomogeneous degree distributions but also nonvanishing clustering and small-worldness observed in many real-world networks, this ensemble attracted significant research attention in mathematics and TCS, where many basic and advanced properties of random hyperbolic graphs have been (re)derived rigorously, see for instance [106, 125–135].

In neuroscience, geometric navigation discussed above offers a possible explanation and a mechanism for the routing of information in the brain. This hypothesis has been investigated at different depths from different angles [136–145]. Yet, geometric navigation is effective only when the network topology is congruent with the underlying latent geometry so that following geodesic paths in the latent space is equivalent to navigating through topological shortest paths. This seems to be the case for the brain [104], well described by the $\mathbb{S}^1/\mathbb{H}^2$ geometric network model, where the same connectivity law rules short and long range connections and operates between brain regions at different length scales [74]. This suggests that simplicity is one of the organizing principles of the large-scale self-similar architecture of human structural brain. Moreover, the multiscale self-similarity of brain connectomes may offer an

advantageous architecture for decentralized navigation purposes [103]. The implications are varied and can be substantial for fundamental debates, like whether the brain is working near a critical point, and for applications including advanced tools to simplify the digital reconstruction and simulation of the brain.

At the same time, primarily after [146], hyperbolic spaces have ignited vigorous research activity in machine learning in many different settings and tasks including embedding graphs and other data, such as images and texts, as well as in the design of neural networks, attention networks, knowledge graphs, and matters alike, with applications ranging from data classification, image recognition, and natural language processing, to link prediction and scalable recommender systems [147–157]. Overall, the main flavor of these results confirms one of the main points in [18]: compared to Euclidean geometry, hyperbolic geometry appears to be a better (embedding space) model for highly heterogeneous networks and other data.

In terms of open questions, one of the most interesting, practically important, but also very challenging one is to generalize latent space network models to temporal networks [158]. Essentially all real-world networks are highly dynamic at different timescales, suggesting that the positions of nodes in the latent space cannot be really fixed but must constantly change. Yet there is no consensus even on the requirements to dynamic latent space network models. The main high-level problem there is that when designing such models there are too many “degrees of freedom”, that is, arbitrary choices can be made, and there are no generally agreed guiding principles concerning what choice is better or worse.

At a more fundamental level, the fact that hyperbolic networks are Lorentz-invariant in the thermodynamic limit suggests to re-examine the role of probabilistic symmetries [159] in the theory of graph limits [160]. Traditionally the main symmetry of interest there has been exchangeability [161]. This is the requirement that the probability of a graph in an ensemble does not depend on how nodes in the graph are labeled, reminiscent of gauge invariance in physics. This requirement is really stringent for deep statistical reasons [161], but it is also easy to appreciate intuitively: if node labels $1 \dots n$ are just random “coordinates” used to represent an otherwise unlabeled graph as an adjacency matrix, then the probability of the graph in the ensemble cannot depend on these meaningless coordinates. The problem is the Aldous-Hoover theorem [162, 163] that says that the thermodynamic limit of any exchangeable sparse graphs is exactly empty. That is why different notions of exchangeability-like probabilistic symmetries have been recently investigated for sparse graph limits [164–167]. Because of the Aldous-Hoover theorem, they all depart from the $1 \dots n$ “coordinate system” for node labels, and rely on different systems of node or edge labels. The Lorentz invariance of hyperbolic networks suggests that the labels of nodes can be indeed their coordinates in a latent space, with exchangeability replaced by invariance with

respect to the space isometries. The hope is that such ensembles may have some interesting and tractable thermodynamic limits.

One of the most fundamental open questions concerns geometrogenesis, that is, the emergence of geometries independent of the background. Geometrogenesis is strongly related to non-perturbative approaches to quantum gravity. In Loop Quantum Gravity (LQG) a basis of states is provided by spin networks which have support on a graph, determining a sort of quantum geometry where the *intrinsic* geometry – consisting of quanta of space – is discrete and the *extrinsic* curvature is fuzzy because of the Heisenberg’s uncertainty principle [168]. However, a main challenge is to assign a classical geometrical interpretation to such states, while recent advances in this direction are based on operators which quantize both scalar and mean curvature when spin network edges run within the surfaces of the quantized geometry [169]. In Quantum Graphity, space is considered as a dynamical graph evolving under the action of a Hamiltonian [45] while in Causal Dynamical Triangulation (CDT) [170] a non-perturbative path integral approach is used to build a connection with Hovrava-Lifshitz gravity in 2+1 dimensions [171]. Spectral dimension, defined as the scaling exponent of the average return probability of diffusion processes (e.g., random walks), is used in CDT to measure the effective dimension of the underlying geometry [172] and can provide an interesting bridge with geometries induced by network-driven processes, where one expects that it characterizes the underlying diffusion manifold. More recently, a model where random graphs dynamically self-assemble into discrete manifold structures has been proposed as an alternative to approaches based on simplicial complexes and Regge calculus. The Ollivier curvature, defined for generic graphs and similar in spirit to Ricci curvature, is used to discretize the Euclidean Einstein-Hilbert action and to provide a new ground for emergent time mechanisms [173].

From a network science perspective, a step forward has been made in [41, 42, 174–176] by defining models of growing random graphs with simplicial complexes as fundamental building blocks. Interestingly, in a wide range of parameters, these models lead to an effective preferential attachment and, thus, heterogeneous degree distributions [174]. Besides, the growth process can be mapped into a tree, inducing an emergent hyperbolic geometry in the resulting graphs [176]. Formulating networks in terms of simplicial complexes also allows the application of persistent homology methods [177] boosting the field of Topological Data Analysis [178] in algebraic topology. Persistent homology relies on a filtration of the simplicial complex to measure topological features that recur over multiple scales and are thus more likely to represent true features of the underlying space. It has been applied to a variety of problems, including spreading processes on networks [31] and the detection of geometric structure

in neural activity [179].

While the results on observable and latent geometries of networks are well established, the geometry of network-driven processes is in its infancy, with promising theoretical developments and important applications to different fields. From the global spread of rumors and opinions in socio-technical systems to the global spread of innovations and epidemics, combining dynamics with the self-similar structure of complex networks and their latent geometry results in heterogeneous processes which cannot be easily understood when investigated in the Euclidean space where they are often embedded. However, when the same dynamical processes are analyzed through the lens of the geometries they induce, one often discovers simple and elegant arguments to better understand the complex spatio-temporal patterns observed in a broad spectrum of complex systems. These results make geometries induced by network-driven processes perhaps the most suitable frameworks for a range of practical applications, from predicting the time course of dynamics for forecasting and control of spreading processes to locating their origin. Indeed, diffusion geometry defines a class of models that have the desirable advantage of being mathematically tractable and can be easily interpreted.

The research program for the future is broad, with many open challenges of theoretical and practical relevance. As the topological organization of empirical complex systems can be characterized in terms of hierarchies [180, 181] and mesoscale structures such as bow-tie [182, 183], k -cores [184, 185] and core-periphery [186, 187], it will be interesting to identify and characterize their functional counterparts in terms of diffusion geometry. Here, the main problem is to define mesoscale objects such as functional giant components and functional cores. At a more fundamental level, the development of RG techniques in the space induced by diffusion distances is highly challenging, but could shed light on the self-similar nature of dynamical processes on the top of a complex network and would open the doors to the analysis of coexisting temporal scales due to the interplay between structure and dynamics.

Finally, a natural development of geometries induced by network-driven processes is the identification and characterization of a more general framework where diffusive dynamics are replaced by more complex ones. This advance would improve our understanding of complex dynamical processes and has the potential to enhance the control and forecasting of the evolution of empirical systems.

Taken together, the advances of network geometry offer a new theoretical framework to gain new insights about the fundamental principles underlying complex systems and, more generally, the physical reality. It is not excluded that current results and future advances on this subject might cross-fertilize with other physics fields.

-
- [1] Cimini, G. *et al.* The statistical physics of real-world networks. *Nature Reviews Physics* **1**, 58 (2019).
- [2] Watts, D. J. & Strogatz, S. H. Collective Dynamics of “Small-World” Networks. *Nature* **393**, 440–442 (1998).
- [3] Barabási, A.-L. & Albert, R. Emergence of Scaling in Random Networks. *Science* **286**, 509–512 (1999).
- [4] Ravasz, E., Somera, A. L., Mongru, D. A., Oltvai, Z. N. & Barabási, A.-L. Hierarchical Organization of Modularity in Metabolic Networks. *Science* **297**, 1551–1555 (2002).
- [5] Dorogovtsev, S. N., Goltsev, A. V. & Mendes, J. F. F. Critical phenomena in complex networks. *Rev Mod Phys* **80**, 1275–1335 (2008).
- [6] Gao, J., Buldyrev, S. V., Stanley, H. E. & Havlin, S. Networks formed from interdependent networks. *Nature Physics* **8**, 40 (2012).
- [7] D’Souza, R. M. & Nagler, J. Anomalous critical and supercritical phenomena in explosive percolation. *Nature Physics* **11**, 531 (2015).
- [8] Gao, J., Barzel, B. & Barabási, A.-L. Universal resilience patterns in complex networks. *Nature* **530**, 307–312 (2016).
- [9] Bianconi, G. Interdisciplinary and physics challenges of network theory. *Europhys Lett* **111**, 56001 (2015).
- [10] Estrada, E. *The structure of complex networks: theory and applications* (Oxford University Press, 2012).
- [11] Song, C., Havlin, S. & Makse, H. A. Self-similarity of complex networks. *Nature* **433**, 392–395 (2005).
- [12] Gallos, L. K., Song, C., Havlin, S. & Makse, H. A. Scaling theory of transport in complex biological networks. *PNAS* **104**, 7746–51 (2007).
- [13] Condamin, S., Bénichou, O., Tejedor, V., Voituriez, R. & Klafter, J. First-passage times in complex scale-invariant media. *Nature* **450**, 77 (2007).
- [14] Radicchi, F., Ramasco, J., Barrat, A. & Fortunato, S. Complex Networks Renormalization: Flows and Fixed Points. *Phys Rev Lett* **101**, 3–6 (2008).
- [15] Rozenfeld, H. D., Song, C. & Makse, H. A. Small-World to Fractal Transition in Complex Networks: A Renormalization Group Approach. *Phys Rev Lett* **104**, 1–4 (2010).
- [16] Song, C., Havlin, S. & Makse, H. A. Origins of fractality in the growth of complex networks. *Nature Physics* **2**, 275–281 (2006).
- [17] Serrano, M. A., Krioukov, D. & Boguñá, M. Self-similarity of complex networks and hidden metric spaces. *Physical Review Letters* **100**, 078701 (2008).
- [18] Krioukov, D., Papadopoulos, F., Kitsak, M., Vahdat, A. & Boguñá, M. Hyperbolic geometry of complex networks. *Phys Rev E* **82**, 036106 (2010).
- [19] Boguñá, M., Krioukov, D. & Claffy, K. C. Navigability of complex networks. *Nat Phys* **5**, 74–80 (2009).
- [20] Gulyás, A., Bíró, J. J., Kőrösi, A., Rétvári, G. & Krioukov, D. Navigable networks as Nash equilibria of navigation games. *Nat Commun* **6**, 7651 (2015).
- [21] Zuev, K., Boguñá, M., Bianconi, G. & Krioukov, D. Emergence of Soft Communities from Geometric Preferential Attachment. *Sci Rep* **5**, 9421 (2015).
- [22] García-Pérez, G., Serrano, M. Á. & Boguñá, M. Soft Communities in Similarity Space. *J Stat Phys* **173**, 775–782 (2018).
- [23] García-Pérez, G., Boguñá, M., Allard, A. & Serrano, M. Á. The hidden hyperbolic geometry of international trade: World Trade Atlas 1870-2013. *Sci Rep* **6**, 33441 (2016).
- [24] García-Pérez, G., Boguñá, M. & Serrano, M. Á. Multiscale unfolding of real networks by geometric renormalization. *Nature Physics* **14**, 583–589 (2018).
- [25] Papadopoulos, F., Kitsak, M., Serrano, M. Á., Boguñá, M. & Krioukov, D. Popularity versus similarity in growing networks. *Nature* **489**, 537–540 (2012).
- [26] Zuev, K., Papadopoulos, F. & Krioukov, D. Hamiltonian dynamics of preferential attachment. *J Phys A Math Theor* **49**, 105001 (2016).
- [27] Zheng, M., García-Pérez, G. & Serrano, M. B. Geometric origins of self-similarity in the evolution of real networks (2019). 1912.00704.
- [28] Krioukov, D. & Ostilli, M. Duality between equilibrium and growing networks. *Phys Rev E* **88**, 022808 (2013).
- [29] Coifman, R. R. *et al.* Geometric diffusions as a tool for harmonic analysis and structure definition of data: Diffusion maps. *Proceedings of the national academy of sciences* **102**, 7426–7431 (2005).
- [30] Brockmann, D. & Helbing, D. The Hidden Geometry of Complex, Network-Driven Contagion Phenomena. *Science* **342**, 1337–1342 (2013).
- [31] Taylor, D. *et al.* Topological data analysis of contagion maps for examining spreading processes on networks. *Nature communications* **6**, 7723 (2015).
- [32] De Domenico, M. Diffusion geometry unravels the emergence of functional clusters in collective phenomena. *Physical Review Letters* **118**, 168301 (2017).
- [33] Hens, C., Harush, U., Haber, S., Cohen, R. & Barzel, B. Spatiotemporal signal propagation in complex networks. *Nature Physics* **1** (2019).
- [34] Gromov, M. *Hyperbolic Groups*, vol. 8 of *Math Sci Res Inst Publ*, 75–263 (Springer, New York, 1987).
- [35] Lin, Y., Lu, L. & Yau, S.-T. Ricci curvature of graphs. *Tohoku Mathematical Journal, Second Series* **63**, 605–627 (2011).
- [36] Higuchi, Y. Combinatorial curvature for planar graphs. *J Graph Theory* **38**, 220–229 (2001).
- [37] Aste, T., Dimatteo, T. & Hyde, S. Complex networks on hyperbolic surfaces. *Physica A* **346**, 20–26 (2005).
- [38] Robles-Kelly, A. & Hancock, E. R. A riemannian approach to graph embedding. *Pattern Recognition* **40**, 1042–1056 (2007).
- [39] Majid, S. Noncommutative riemannian geometry on graphs. *Journal of Geometry and Physics* **69**, 74–93 (2013).
- [40] Franzosi, R., Felice, D., Mancini, S. & Pettini, M. Riemannian-geometric entropy for measuring network complexity. *Phys Rev E* **93**, 062317 (2016).
- [41] Wu, Z., Menichetti, G., Rahmede, C. & Bianconi, G. Emergent Complex Network Geometry. *Sci Rep* **5**, 10073 (2015).
- [42] Mulder, D. & Bianconi, G. Network Geometry and Complexity. *J Stat Phys* (2018).
- [43] Rideout, D. & Walden, P. Spacelike distance from discrete causal order. *Class Quantum Gravity* **26**, 155013 (2009).
- [44] Dowker, F. Spacetime discreteness, Lorentz invariance and locality. *J Phys Conf Ser* **306**, 012016 (2011).
- [45] Konopka, T., Markopoulou, F. & Severini, S. Quantum graphity: A model of emergent locality. *Physical Review D* **77**, 104029 (2008).
- [46] Ambjørn, J., Jurkiewicz, J. & Loll, R. The Spec-

- tral Dimension of the Universe is Scale Dependent. *Physical Review Letters* **95**, 171301 (2005).
- [47] Song, C., Gallos, L. K., Havlin, S. & Makse, H. A. How to calculate the fractal dimension of a complex network: the box covering algorithm. *Journal of Statistical Mechanics: Theory and Experiment* **2007**, P03006 (2007).
- [48] García-Pérez, G., Boguñá, M. & Serrano, M. Á. Multiscale unfolding of real networks by geometric renormalization. *Nat Phys* **14**, 583–589 (2018).
- [49] Feder, J. *Fractals* (Springer Science & Business Media, 2013).
- [50] Cardy, J. *Scaling and renormalization in statistical physics*, vol. 5 (Cambridge university press, 1996).
- [51] Lesne, A. & Laguës, M. *Scale invariance: From phase transitions to turbulence* (Springer Science & Business Media, 2011).
- [52] Cohen, R. & Havlin, S. Scale-Free Networks Are Ultrasmall. *Phys Rev Lett* **90**, 058701 (2003).
- [53] Mandelbrot, B. B. *The fractal geometry of nature*, vol. 2 (WH freeman New York, 1982).
- [54] Havlin, S., Trus, B. & Stanley, H. Cluster-growth model for branched polymers that are” chemically linear”. *Physical Review Letters* **53**, 1288 (1984).
- [55] Wilson, K. G. The renormalization group and critical phenomena. *Rev. Mod. Phys.* **55**, 583–600 (1983). URL <http://link.aps.org/doi/10.1103/RevModPhys.55.583>.
- [56] Efrati, E., Wang, Z., Kolan, A. & Kadanoff, L. P. Real-space renormalization in statistical mechanics. *Reviews of Modern Physics* **86**, 647 (2014).
- [57] Gallos, L. K., Song, C. & Makse, H. A. Scaling of degree correlations and its influence on diffusion in scale-free networks. *Physical Review Letters* **100**, 248701 (2008).
- [58] Rozenfeld, H. D., Gallos, L. K., Song, C. & Makse, H. A. Fractal and transfractal scale-free networks. *Encyclopedia of Complexity and Systems Science* 3924–3943 (2009).
- [59] Bunde, A. & Havlin, S. *Fractals and disordered systems* (Springer Science & Business Media, 2012).
- [60] Goh, K.-I., Salvi, G., Kahng, B. & Kim, D. Skeleton and fractal scaling in complex networks. *Physical review letters* **96**, 018701 (2006).
- [61] Kim, J. *et al.* Fractality in complex networks: critical and supercritical skeletons. *Physical Review E* **75**, 016110 (2007).
- [62] Yook, S.-H., Radicchi, F. & Meyer-Ortmanns, H. Self-similar scale-free networks and disassortativity. *Physical Review E* **72**, 045105 (2005).
- [63] Galvão, V. *et al.* Modularity map of the network of human cell differentiation. *Proceedings of the National Academy of Sciences* **107**, 5750–5755 (2010).
- [64] Newman, M. E. J. Modularity and Community Structure in Networks. *Proc Natl Acad Sci USA* **103**, 8577–8582 (2006).
- [65] Fortunato, S. Community detection in graphs. *Phys Rep* **486**, 75–174 (2010).
- [66] Radicchi, F., Barrat, A., Fortunato, S. & Ramasco, J. Renormalization flows in complex networks. *Phys Rev E* **79**, 1–11 (2009).
- [67] Gallos, L. K., Makse, H. A. & Sigman, M. A small world of weak ties provides optimal global integration of self-similar modules in functional brain networks. *Proc Natl Acad Sci* **109**, 2825–30 (2012).
- [68] Jin, Y., Turaev, D., Weinmaier, T., Rattei, T. & Makse, H. A. The evolutionary dynamics of protein-protein interaction networks inferred from the reconstruction of ancient networks. *PLoS one* **8**, e58134 (2013).
- [69] Kleinberg, J. Navigation in a Small World. *Nature* **406**, 845 (2000).
- [70] Viswanathan, G. M. *et al.* Optimizing the success of random searches. *Nature* **401**, 911–4 (1999).
- [71] Nekrashevych, V. *Self-Similar Groups*, vol. 117 of *Mathematical Surveys and Monographs* (American Mathematical Society, Providence, Rhode Island, 2005).
- [72] Buyalo, S. & Schroeder, V. *Elements of Asymptotic Geometry* (European Mathematical Society Publishing House, Zürich, Switzerland, 2007).
- [73] Grigorchuk, R., Nekrashevych, V. & Šunić, Z. *From Self-Similar Groups to Self-Similar Sets and Spectra*, 175–207 (Birkhäuser, Cham, Switzerland, 2015).
- [74] Zheng, M., Allard, A., Hagmann, P. & Serrano, M. A. Geometric renormalization unravels self-similarity of the multiscale human connectome (2019). 1904.11793.
- [75] Boguñá, M., Papadopoulos, F. & Krioukov, D. Sustaining the Internet with hyperbolic mapping. *Nat Commun* **1**, 1–8 (2010).
- [76] Sorokin, A. P. *Social Mobility* (Harper, New York, 1927).
- [77] McFarland, D. D. & Brown, D. J. *Social distance as a metric: A systematic introduction to smallest space analysis*, 213–252 (John Wiley, New York, 1973).
- [78] Hoff, P. D., Raftery, A. E. & Handcock, M. S. Latent Space Approaches to Social Network Analysis. *J Am Stat Assoc* **97**, 1090–1098 (2002).
- [79] Penrose, M. *Random Geometric Graphs* (Oxford University Press, Oxford, 2003).
- [80] Boguñá, M., Krioukov, D., Almagro, P. & Serrano, M. A. Small worlds and clustering in spatial networks (2019). 1909.00226.
- [81] Serrano, M. Á., Krioukov, D. & Boguñá, M. Self-Similarity of Complex Networks and Hidden Metric Spaces. *Phys Rev Lett* **100**, 078701 (2008).
- [82] van der Hoorn, P., Lippner, G. & Krioukov, D. Sparse Maximum-Entropy Random Graphs with a Given Power-Law Degree Distribution. *J Stat Phys* **173**, 806–844 (2018).
- [83] Cannon, J., Floyd, W., Kenyon, R. & Parry, W. *Hyperbolic Geometry*, 59–116 (MSRI, Berkeley, 1997).
- [84] Ratcliffe, J. *Foundations of Hyperbolic Manifolds* (Springer, New York, 2006).
- [85] Maldacena, J. The large N limit of superconformal field theories and supergravity. *Adv Theor Math Phys* **2**, 231–252 (1998).
- [86] Krioukov, D. *et al.* Network Cosmology. *Sci Rep* **2**, 793 (2012).
- [87] Allard, A., Serrano, M. Á., García-Pérez, G. & Boguñá, M. The geometric nature of weights in real complex networks. *Nat Commun* **8**, 14103 (2017).
- [88] Kleineberg, K.-K., Boguñá, M., Ángeles Serrano, M. & Papadopoulos, F. Hidden geometric correlations in real multiplex networks. *Nat Phys* **12**, 1076–1081 (2016).
- [89] Kleineberg, K.-K., Buzna, L., Papadopoulos, F., Boguñá, M. & Serrano, M. A. Geometric Correlations Mitigate the Extreme Vulnerability of Multiplex Networks against Targeted Attacks. *Physical Review Letters* **118**, 218301 (2017).
- [90] Muscoloni, A. & Cannistraci, C. V. A nonuniform popularity-similarity optimization (nPSO) model to efficiently generate realistic complex networks with communities. *New J Phys* **20**, 052002 (2018).
- [91] Papadopoulos, F., Psomas, C. & Krioukov, D. Network Mapping by Replaying Hyperbolic Growth. *IEEE/ACM Trans Netw* **23**, 198–211 (2015).

- [92] Papadopoulos, F., Aldecoa, R. & Krioukov, D. Network geometry inference using common neighbors. *Phys Rev E* **92**, 022807 (2015).
- [93] Wang, Z., Li, Q., Jin, F., Xiong, W. & Wu, Y. Hyperbolic mapping of complex networks based on community information. *Phys A Stat Mech its Appl* **455**, 104–119 (2016).
- [94] Wang, Z., Wu, Y., Li, Q., Jin, F. & Xiong, W. Link prediction based on hyperbolic mapping with community structure for complex networks. *Phys A Stat Mech its Appl* **450**, 609–623 (2016).
- [95] Alanis-Lobato, G., Mier, P. & Andrade-Navarro, M. A. Efficient embedding of complex networks to hyperbolic space via their Laplacian. *Sci Rep* **6**, 30108 (2016).
- [96] Alanis-Lobato, G., Mier, P. & Andrade-Navarro, M. A. Manifold learning and maximum likelihood estimation for hyperbolic network embedding. *Appl Netw Sci* **1**, 10 (2016).
- [97] Muscoloni, A., Thomas, J. M., Ciucci, S., Bianconi, G. & Cannistraci, C. V. Machine learning meets complex networks via coalescent embedding in the hyperbolic space. *Nat Commun* **8**, 1615 (2017).
- [98] Blasius, T., Friedrich, T., Krohmer, A. & Laue, S. Efficient Embedding of Scale-Free Graphs in the Hyperbolic Plane. *IEEE/ACM Trans Netw* **26**, 920–933 (2018).
- [99] Garcia-Perez, G., Allard, A., Serrano, M. A. & Boguna, M. Mercator: uncovering faithful hyperbolic embeddings of complex networks. *New Journal of Physics* (2019).
- [100] Serrano, M. Á., Boguñá, M. & Sagués, F. Uncovering the hidden geometry behind metabolic networks. *Mol Biosyst* **8**, 843 (2012).
- [101] Kleineberg, K.-K. Metric clusters in evolutionary games on scale-free networks. *Nat Commun* **8**, 1888 (2017).
- [102] Voitalov, I., Aldecoa, R., Wang, L. & Krioukov, D. Geohyperbolic Routing and Addressing Schemes. *ACM SIGCOMM Comput Commun Rev* **47**, 11–18 (2017).
- [103] Zheng, M., Allard, A., Hagmann, P. & Serrano, M. . Geometric renormalization unravels self-similarity of the multiscale human connectome (2019). 1904.11793.
- [104] Allard, A. & Serrano, M. A. Navigable maps of structural brain networks across species (2018). 1801.06079.
- [105] Korman, A. & Peleg, D. *Dynamic Routing Schemes for General Graphs*, vol. 4051 of *Lecture Notes in Computer Science*, 619–630 (Springer, 2006).
- [106] Bringmann, K., Keusch, R., Lengler, J., Maus, Y. & Molla, A. R. Greedy Routing and the Algorithmic Small-World Phenomenon. In *Proc ACM Symp Princ Distrib Comput - Pod '17* (2017).
- [107] Boguñá, M. & Krioukov, D. Navigating Ultrasmall Worlds in Ultrashort Time. *Phys Rev Lett* **102**, 058701 (2009).
- [108] Serrano, M. Á., Krioukov, D. & Boguñá, M. Percolation in Self-Similar Networks. *Phys Rev Lett* **106**, 048701 (2011).
- [109] Pastor-Satorras, R. & Vespignani, A. Epidemic spreading in scale-free networks. *Phys Rev Lett* **86**, 3200–3203 (2001).
- [110] Dorogovtsev, S. N., Goltsev, A. V. & Mendes, J. F. F. Ising model on networks with an arbitrary distribution of connections. *Phys. Rev. E* **66**, 016104 (2002).
- [111] Leo P., K. *Statistical Physics: Statics, Dynamics and Renormalization* (World Scientific, Singapore, 2000).
- [112] De Domenico, M. Diffusion Geometry Unravels the Emergence of Functional Clusters in Collective Phenomena. *Phys Rev Lett* **118**, 168301 (2017).
- [113] Estrada, E. Complex networks in the euclidean space of communicability distances. *Physical Review E* **85**, 066122 (2012).
- [114] Estrada, E., Hatano, N. & Benzi, M. The physics of communicability in complex networks. *Physics reports* **514**, 89–119 (2012).
- [115] Akbarzadeh, M. & Estrada, E. Communicability geometry captures traffic flows in cities. *Nature Human Behaviour* **2**, 645 (2018).
- [116] Estrada, E. Communicability geometry of multiplexes. *New Journal of Physics* (2018).
- [117] De Domenico, M., Granell, C., Porter, M. A. & Arenas, A. The physics of spreading processes in multilayer networks. *Nature Physics* **12**, 901–906 (2016).
- [118] Iannelli, F., Koher, A., Brockmann, D., Hoevel, P. & Sokolov, I. M. Effective Distances for Epidemics Spreading on Complex Networks. *Physical Review E* **95**, 012313 (2016).
- [119] Masuda, N., Porter, M. A. & Lambiotte, R. Random walks and diffusion on networks. *Physics reports* **716**, 1–58 (2017).
- [120] Bertagnolli, G., Agostinelli, C. & Domenico, M. D. Network depth: identifying median and contours in complex networks. *Journal of Complex Networks* (2019).
- [121] Gallos, L. K., Song, C. & Makse, H. A. A review of fractality and self-similarity in complex networks. *Physica A: Statistical Mechanics and its Applications* **386**, 686–691 (2007).
- [122] Villani, C. *Optimal transport: old and new*, vol. 338 (Springer Science & Business Media, 2008).
- [123] Furstenberg, H. *Ergodic theory and fractal geometry*, vol. 120 (American Mathematical Society, 2014).
- [124] Furstenberg, H. & Weiss, B. Markov processes and ramsey theory for trees. *Combinatorics, Probability and Computing* **12**, 547–563 (2003).
- [125] Gugelmann, L., Panagiotou, K. & Peter, U. *Random Hyperbolic Graphs: Degree Sequence and Clustering*, 573–585 (Springer, Berlin, Heidelberg, 2012).
- [126] Fountoulakis, N. On a geometrization of the ChungLu model for complex networks. *J Complex Networks* **3**, 361–387 (2015).
- [127] Candellero, E. & Fountoulakis, N. Clustering and the Hyperbolic Geometry of Complex Networks. *Internet Math* **12**, 2–53 (2016).
- [128] Bode, M., Fountoulakis, N. & Müller, T. The probability of connectivity in a hyperbolic model of complex networks. *Random Struct Algor* **49**, 65–94 (2016).
- [129] Abdullah, M. A., Fountoulakis, N. & Bode, M. Typical distances in a geometric model for complex networks. *Internet Math* (2017).
- [130] Bläsius, T., Friedrich, T. & Krohmer, A. Cliques in Hyperbolic Random Graphs. *Algorithmica* **80**, 2324–2344 (2018).
- [131] Fountoulakis, N. & Müller, T. Law of large numbers for the largest component in a hyperbolic model of complex networks. *Ann Appl Probab* **28**, 607–650 (2018).
- [132] Friedrich, T. & Krohmer, A. On the Diameter of Hyperbolic Random Graphs. *SIAM J Discret Math* **32**, 1314–1334 (2018).
- [133] Kiwi, M. & Mitsche, D. Spectral gap of random hyperbolic graphs and related parameters. *Ann Appl Probab* **28**, 941–989 (2018).
- [134] Bringmann, K., Keusch, R. & Lengler, J. Geometric

- inhomogeneous random graphs. *Theor Comput Sci* **760**, 35–54 (2019).
- [135] Müller, T. & Staps, M. The diameter of KPKVB random graphs. *Adv Appl Probab* **51**, 358–377 (2019).
- [136] van den Heuvel, M. P., Kahn, R. S., Goni, J. & Sporns, O. High-cost, high-capacity backbone for global brain communication. *Proc Natl Acad Sci* **109**, 11372–11377 (2012).
- [137] Goñi, J. *et al.* Exploring the Morphospace of Communication Efficiency in Complex Networks. *PLoS One* **8**, e58070 (2013).
- [138] Fornito, A., Zalesky, A. & Breakspear, M. Graph analysis of the human connectome: Promise, progress, and pitfalls. *Neuroimage* **80**, 426–444 (2013).
- [139] Mišić, B., Sporns, O. & McIntosh, A. R. Communication Efficiency and Congestion of Signal Traffic in Large-Scale Brain Networks. *PLoS Comput Biol* **10**, e1003427 (2014).
- [140] Roberts, J. A. *et al.* The contribution of geometry to the human connectome. *Neuroimage* **124**, 379–393 (2016).
- [141] Avena-Koenigsberger, A. *et al.* Path ensembles and a tradeoff between communication efficiency and resilience in the human connectome. *Brain Struct Funct* **222**, 603–618 (2017).
- [142] Seguin, C., van den Heuvel, M. P. & Zalesky, A. Navigation of brain networks. *Proc Natl Acad Sci* **115**, 6297–6302 (2018).
- [143] Tadić, B., Andjelković, M. & Šuvakov, M. Origin of Hyperbolicity in Brain-to-Brain Coordination Networks. *Front Phys* **6** (2018).
- [144] Avena-Koenigsberger, A. *et al.* A spectrum of routing strategies for brain networks. *PLOS Comput Biol* **15**, e1006833 (2019).
- [145] Wang, X. *et al.* Synchronization lag in post stroke: relation to motor function and structural connectivity. *Netw Neurosci* **3**, 1121–1140 (2019).
- [146] Nickel, M. & Kiela, D. Poincaré Embeddings for Learning Hierarchical Representations. In *Adv neural Inf Process Syst* (2017).
- [147] Dhingra, B., Shallue, C. J., Norouzi, M., Dai, A. M. & Dahl, G. E. Embedding Text in Hyperbolic Spaces. In *NAACL HLT* (2018).
- [148] Ganea, O.-E., Bécigneul, G. & Hofmann, T. Hyperbolic Entailment Cones for Learning Hierarchical Embeddings. In *Int Conf Mach Learn* (2018).
- [149] Ganea, O.-E., Bécigneul, G. & Hofmann, T. Hyperbolic Neural Networks. In *Adv Neural Inf Process Syst* (2018).
- [150] Nickel, M. & Kiela, D. Learning Continuous Hierarchies in the Lorentz Model of Hyperbolic Geometry. In *Int Conf Mach Learn* (2018).
- [151] Ovinnikov, I. Poincaré Wasserstein Autoencoder. In *Adv Neural Inf Process Syst* (2018).
- [152] Sala, F. *et al.* Representation Tradeoffs for Hyperbolic Embeddings. In *Int Conf Mach Learn* (2018).
- [153] Gulcehre, C. *et al.* Hyperbolic Attention Networks. In *Int Conf Learn Represent* (2019).
- [154] Chami, I., Ying, R., Ré, C. & Leskovec, J. Hyperbolic Graph Convolutional Neural Networks (2019). 1910.12933.
- [155] Liu, Q., Nickel, M. & Kiela, D. Hyperbolic Graph Neural Networks. In *Adv Neural Inf Process Syst* (2019).
- [156] Suzuki, A., Wang, J., Tian, F., Nitanda, A. & Yamaniishi, K. Hyperbolic Ordinal Embedding. In *Proc Mach Learn Res* (2019).
- [157] Tifrea, A., Bécigneul, G. & Ganea, O.-E. Poincaré GloVe: Hyperbolic Word Embeddings. In *Int Conf Learn Represent* (2019).
- [158] Holme, P. & Saramäki, J. Temporal networks. *Physics reports* **519**, 97–125 (2012).
- [159] Kallenberg, O. *Probabilistic Symmetries and Invariance Principles* (Springer, New York, 2005).
- [160] Lovász, L. *Large Networks and Graph Limits* (American Mathematical Society, Providence, RI, 2012).
- [161] Orbanz, P. & Roy, D. M. Bayesian models of graphs, arrays and other exchangeable random structures. *IEEE Trans Pattern Anal Mach Intell* **37**, 437–461 (2015).
- [162] Aldous, D. J. Representations for partially exchangeable arrays of random variables. *J Multivar Anal* **11**, 581–598 (1981).
- [163] Hoover, D. N. Relations on Probability Spaces and Arrays of Random Variables. Tech. Rep., Institute for Advanced Study, Princeton, NJ (1979).
- [164] Caron, F. & Fox, E. B. Sparse graphs using exchangeable random measures. *J R Stat Soc Ser B (Statistical Methodol)* **79**, 1295–1366 (2017).
- [165] Veitch, V. & Roy, D. M. The Class of Random Graphs Arising from Exchangeable Random Measures (2015). 1512.03099.
- [166] Borgs, C., Chayes, J. T., Cohn, H. & Zhao, Y. An L^p theory of sparse graph convergence I: Limits, sparse random graph models, and power law distributions. *Trans Am Math Soc* **372**, 3019–3062 (2019).
- [167] Janson, S. On Edge Exchangeable Random Graphs. *J Stat Phys* 1–37 (2017).
- [168] Rovelli, C. & Speziale, S. On the geometry of loop quantum gravity on a graph. *Phys Rev D* **82**, 44018 (2010).
- [169] Grüber, D., Sahlmann, H. & Zilker, T. Geometry and entanglement entropy of surfaces in loop quantum gravity. *Physical Review D* **98**, 066009 (2018).
- [170] Ambjørn, J., Jordan, S., Jurkiewicz, J. & Loll, R. Second-Order Phase Transition in Causal Dynamical Triangulations. *Physical Review Letters* **107**, 211303 (2011).
- [171] Sotiriou, T. P., Visser, M. & Weinfurtner, S. Spectral Dimension as a Probe of the Ultraviolet Continuum Regime of Causal Dynamical Triangulations. *Physical Review Letters* **107**, 131303 (2011).
- [172] Loll, R. Quantum gravity from causal dynamical triangulations: a review. *Classical and Quantum Gravity* **In press** (2019).
- [173] Kelly, C., Trugenberger, C. A. & Biancalana, F. Self-assembly of geometric space from random graphs. *Class Quantum Gravity* **36**, 125012 (2019).
- [174] Bianconi, G. & Rahmede, C. Complex Quantum Network Manifolds in Dimension $d > 2$ are Scale-Free. *Sci Rep* **5**, 13979 (2015).
- [175] Bianconi, G. & Rahmede, C. Network geometry with flavor: From complexity to quantum geometry. *Phys Rev E* **93**, 032315 (2016).
- [176] Bianconi, G. & Rahmede, C. Emergent Hyperbolic Network Geometry. *Sci Rep* **7**, 41974 (2017).
- [177] Aktas, M. E., Akbas, E. & El Fatmaoui, A. Persistence homology of networks: methods and applications. *Applied Network Science* **4**, 61 (2019).
- [178] Patania, A., Vaccarino, F. & Petri, G. Topological analysis of data. *EPJ Data Science* **6**, 7 (2017).
- [179] Giusti, C., Pastalkova, E., Curto, C. & Itskov, V. Clique topology reveals intrinsic geometric structure in neural correlations. *Proceedings of the National Academy of Sciences* **112**, 13455–13460 (2015).
- [180] Ravasz, E. & Barabási, A.-L. Hierarchical organization in complex networks. *Phys Rev E* **67**, 026112 (2003).

- [181] Corominas-Murtra, B., Goñi, J., Solé, R. V. & Rodríguez-Caso, C. On the origins of hierarchy in complex networks. *Proceedings of the National Academy of Sciences* **110**, 13316–13321 (2013).
- [182] Newman, M. E. J., Strogatz, S. H. & Watts, D. J. Random Graphs with Arbitrary Degree Distributions and Their Applications. *Phys Rev E* **64**, 26118 (2001).
- [183] Dorogovtsev, S. N., Mendes, J. F. F. & Samukhin, A. N. Giant strongly connected component of directed networks. *Physical Review E* **64**, 025101 (2001).
- [184] Seidman, S. B. Network structure and minimum degree. *Social networks* **5**, 269–287 (1983).
- [185] Dorogovtsev, S. N., Goltsev, A. V. & Mendes, J. F. F. K-core organization of complex networks. *Physical review letters* **96**, 040601 (2006).
- [186] Holme, P. Core-periphery organization of complex networks. *Physical Review E* **72**, 046111 (2005).
- [187] Rombach, M. P., Porter, M. A., Fowler, J. H. & Mucha, P. J. Core-periphery structure in networks. *SIAM Journal on Applied mathematics* **74**, 167–190 (2014).
- [188] The approximation holds for a fraction of node pairs that converges to 1 in the thermodynamic limit [18]